Article

Current Biology

Mate Selection in Self-Compatible Wild Tobacco Results from Coordinated Variation in Homologous Self-Incompatibility Genes

Graphical Abstract

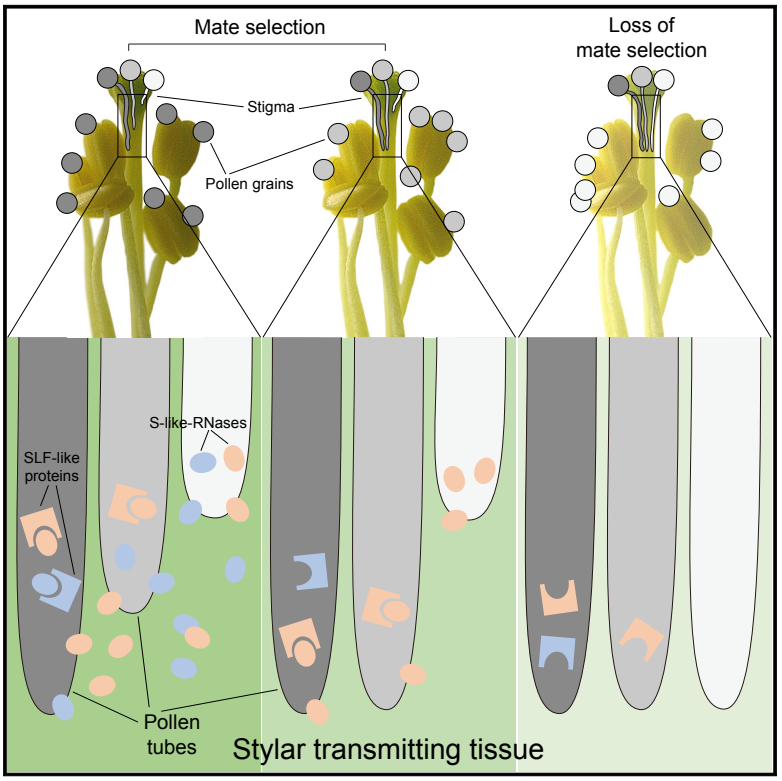

Authors

Han Guo, Rayko Halitschke, Natalie Wielsch, Klaus Gase, Ian T. Baldwin

Correspondence

baldwin@ice.mpg.de

In Brief

Robust and coordinated abundance variations were found in homologous self-incompatibility genes among self-compatible *Nicotiana attenuata* accessions, which accounts for the species' polyandrous mate selection system. By describing the mechanisms of mate selection, Guo et al. provide the tools to evaluate if the mate choices of plants are adaptive.

Highlights

- Molecular basis of polyandrous mate selection in self-compatible wild tobacco
- Coordinated abundance variations of style and pollen elements among accessions
- Remnants of SI mechanisms have been repurposed by evolution for mate selection

Guo et al., 2019, Current Biology *29*, 2020–2030
June 17, 2019
https://doi.org/10.1016/j.cub.2019.05.042

CellPress

CellPress

Current Biology
Article

Mate Selection in Self-Compatible Wild Tobacco Results from Coordinated Variation in Homologous Self-Incompatibility Genes

Han Guo,[1] Rayko Halitschke,[1] Natalie Wielsch,[2] Klaus Gase,[1] and Ian T. Baldwin[1,3,*]
[1]Department of Molecular Ecology, Max Planck Institute for Chemical Ecology, Hans-Knoell-Strasse 8, DE-07745 Jena, Germany
[2]Research Group Mass Spectrometry/Proteomics, Max Planck Institute for Chemical Ecology, Hans-Knoell-Strasse 8, DE-07745 Jena, Germany
[3]Lead Contact
*Correspondence: baldwin@ice.mpg.de
https://doi.org/10.1016/j.cub.2019.05.042

SUMMARY

In flowering plants, intraspecific mate preference is frequently related to mating systems: the rejection of self pollen in self-incompatible (SI) plants that prevents inbreeding is one of the best described examples. However, in other mating systems, more nuanced patterns of pollen rejection occur. In the self-compatible (SC) *Nicotiana attenuata*, in which SI is not found and all crosses are compatible, certain pollen genotypes are consistently selected in mixed pollinations. However, the molecular mechanisms of this polyandrous mate selection remain unknown. Style-expressed *NaS-like-RNases* and pollen-expressed *NaSLF-like* genes, homologous to SI factors in Solanaceae, were identified and examined for a role in *N. attenuata*'s mate selection. A comparison of two *NaS-like-RNases* and six *NaSLF-like* genes among 26 natural accessions revealed specific combinations of co-expression and direct protein-protein interactions. To evaluate their role in mate selection, we silenced the expression of specific NaS-like-RNases and NaSLF-like proteins and conducted diagnostic binary mixed pollinations and mixed pollinations with 14 different non-self pollen donors. Styles expressing particular combinations of NaS-like-RNases selected mates from plants with corresponding NaS-like-RNase expression patterns, while styles lacking NaS-like-RNase expression were non-selective in their fertilizations, which reflected the genotype ratios of pollen mixtures deposited on the stigmas. DNA methylation could account for some of the observed variation in stylar NaS-like-RNase patterns. We conclude that the S-RNase-SLF recognition mechanism plays a central role in polyandrous mate selection in this self-compatible species. These results suggest that after the SI-SC transition, natural variation of SI homologous genes was repurposed to mediate intraspecific mate selection.

INTRODUCTION

Flowering plants recognize and select particular conspecific mates in diverse patterns depending on the plant's mating system, which can differ in preference (e.g., self or non-self pollen) and mechanism (e.g., pollen rejection or competition). In obligate outcrossing populations of self-incompatible (SI) species, individuals reject self pollen that prevents inbreeding and promotes outcrossing [1, 2]. In the Solanaceae, SI is controlled by a single multi-haplotype *S*-locus. Each *S*-haplotype carries both pollen- and pistil-specific determinants (*S*-determinants), and discrimination between self and non-self is mediated by specific molecular interactions between pollen and pistil *S*-determinants [2, 3]. The pistil *S*-determinant encodes an extracellular RNase (S-RNase) acting as a cytotoxic factor that inhibits the growth of self pollen tubes [4–7]. The pollen *S*-determinant is an F-box protein, named *S*-locus F-box (SLF) [8–11], a component of an SCF (Skp1-Cullin1-F-box) complex that degrades non-self S-RNases and allows for the growth of compatible pollen tubes and their fertilization success [12–16]. The recognition between pistil and pollen *S*-determinants is thought to be a collaborative non-self-recognition process, in which the pollen *S*-determinant consists of multiple *SLF* genes [17]. Each SLF protein interacts specifically with one or more S-RNase proteins of other *S*-haplotypes and allows pollen tubes to grow through most non-self styles in a natural SI population [18, 19].

In *Solanum habrochaites*, pollen rejection is commonly found when styles of SI populations are pollinated by pollen from SC populations, but not vice versa [20]. This has been called intraspecific unilateral incompatibility (UI) [21] and is thought to be related to the SI-SC transition for this species. However, pollen from northern SC populations is also rejected by southern SC populations, suggesting that the outcrossing incompatibility among different SC populations results from multiple independent SI-SC transitions (reviewed in [21]).

Nicotiana attenuata (Solanaceae) is a fully SC diploid native tobacco in which more than 30% of the seeds are produced from opportunistic outcrossing in native populations [22, 23]. The SI-SC transition likely occurred in the ancestral species of *N. attenuata* and three related *Nicotiana* species ~10.8 million years ago (Figure S1A) [24, 25]. All self and non-self pollinations are fully compatible in all tested extant *N. attenuata* populations. This species was shown to have a polyandrous mate selection

system in which self pollen is consistently selected for from binary-genotype mixed pollinations, whereas all self and non-self pollen are equally compatible in single-genotype pollinations [26]. In contrast to the SI and intraspecific UI systems, differences in pollen tube competitive ability rather than pollen tube acceptance are responsible for mate selection, as seed siring success is correlated with differences in pollen tube growth rates between favored and unfavored pollen and primarily occurs within the upper portion of the style and early in the flower's lifespan [26]. However, the mechanisms by which *N. attenuata* recognizes and selects mates among the copious amounts of compatible pollen delivered to the stigma are unknown.

To determine whether SI homologous genes are active in the SC *N. attenuata*, we conducted a genome-wide search and identified two *NaS-like-RNases*, six *NaSLF-like* genes, one *NaSSK1*, and one *NaCUL1*. In contrast to the common SI situation found in other Solanaceous species, where heterozygous individuals harbor many different *S-RNase* alleles, only two non-allelic *NaS-like-RNases* were found in most of the 26 *N. attenuata* natural accessions that we explored. Utilizing the natural variation in *NaS-like-RNase* expression in combination with targeted RNAi-based manipulations of the S-like-RNases and SLF-like proteins, we show that the S-RNase-SLF recognition mechanism plays a central role in mate selection of this SC native tobacco. We conclude that natural variation in homologous SI genes contributes to the selection of mates from mixed pollen loads in *N. attenuata* and discuss potential molecular mechanisms and consequences for the genetic diversity in this SC native tobacco species.

RESULTS

Variation in NaS-like-RNase Abundance Is Correlated with Mate Selection

Although *N. attenuata* is SC, we found two style-specific *ribonuclease* genes (*NaS-like-RNase1* and *2*) (Figures S1B and S1C) by homologous cloning in the genomes of two natural accessions (UT and AZ). *S-like-RNase1* and *2* are homologous to previously described *S-RNase* genes (Figure S1D), which are thought to be a cytotoxic factor blocking growth of self pollen tubes in SI mating systems. To investigate the relationship between S-like-RNases and mate selection in the fully SC species, *N. attenuata*, we characterized stylar protein abundances of S-like-RNase1 and 2 and mate selection phenotypes of four different genotypes after mixture pollinations with equal numbers of self and non-self pollen (Figure 1A). The four natural accessions (AZ, UT, G8, and G2) varied substantially in their stylar S-like-RNase profiles. S-like-RNase1 was abundant in UT and AZ styles, but was not detected in G8 and G2 styles (Figure 1B; Table S1). S-like-RNase2 was also abundant in AZ styles, but only trace amounts of S-like-RNase2 were found in UT styles, while it was not detected in G8 and G2 styles (Figures 1B; Table S1). If S-like-RNases are involved in mate selection, we predicted that the loss of S-like-RNase expression in G8 and G2 styles would result in a loss of mate selection capability in these accessions. We mixed equal numbers of pollen grains from UT and G8 or AZ and G8 to pollinate emasculated flowers of UT and G8 or AZ and G8 plants, respectively. The paternity of seeds resulting from these binary mixture pollinations was genotyped using *N. attenuata trypsin proteinase inhibitor* (*NaTPI*) and dCAPS markers (Figures S1E and S1F; Table S4). While UT and AZ flowers showed a preference for self pollen, G8 flowers did not discriminate between UT:G8 (Figure 1C) or AZ:G8 (Figure 1E) pollen, respectively, in binary mixed pollinations.

A similar experiment (using equal pollen mixtures from UT and G2 or AZ and G2 to pollinate emasculated flowers of UT and G2 or AZ and G2 plants, respectively) showed that although AZ flowers showed a preference for self pollen, G2 flowers did not discriminate between UT:G2 (Figure 1D) or AZ:G2 (Figure 1F) pollen. Interestingly, UT flowers did not prefer self pollen in UT:G2 pollinations (Figure 1D). These observed patterns of seed siring were consistent with a role for S-like-RNases in the mate selection of *N. attenuata*.

NaS-like-RNase1 and 2 Mediate Mate Selection

To further characterize the function of S-like-RNases, we silenced *S-like-RNase1* in UT and AZ and *S-like-RNase2* in AZ by virus-induced gene silencing (VIGS). The VIGS resulted in specific reductions by ~93% and ~94% of S-like-RNase1 abundance in UT and AZ, respectively (Figure 1B; Table S1). Similarly, S-like-RNase2 abundance was specifically reduced by ~89% in AZ (Figure 1B; Table S1). We used equal pollen mixtures from UT and G8 or UT and G2 to pollinate UT *empty vector* control (VIGS-*EV*/UT) or *S-like-RNase1*-silenced lines (VIGS-*SLR1*/UT), respectively. Compared to VIGS-*EV*/UT, we observed a significant reduction of self-preference in the seed siring by UT:G8 pollen mixtures in emasculated flowers of VIGS-*SLR1*/UT plants (Figure 1C), while flowers of both VIGS-*EV*/UT and VIGS-*SLR1*/UT did not discriminate between UT:G2 pollen as inferred from their seed siring ratios (Figure 1D). Similarly, we used equal pollen mixtures of AZ and G8 or AZ and G2 to pollinate emasculated flowers of VIGS-*EV*/AZ, VIGS-*SLR1*/AZ, and VIGS-*SLR2*/AZ plants. Compared to VIGS-*EV*/AZ, silencing *S-like-RNase1* or *2* significantly reduced self-preference in AZ:G8 pollinations (Figure 1E). While emasculated flowers of VIGS-*SLR2*/AZ plants also lost self-preference when pollinated with AZ:G2 pollen, VIGS-*SLR1*/AZ flowers showed similar self-preference in AZ:G2 pollination compared to VIGS-*EV*/AZ (Figure 1F). In summary, these data reveal that both NaS-like-RNase1 and 2 are mate selection factors and their abundances contribute to natural variation in mate selection.

Natural Variation in NaS-like-RNase Abundance Is Highly Correlated with Coding Region Cytosine Methylation

We examined *NaS-like-RNase* copy numbers in the four accessions to explore if a deletion was responsible for the loss of expression. While *S-like-RNase1* was deleted in G2 and G8 (Figure S2A), which is consistent with the loss of expression in the styles of G2 and G8, we found one copy of *S-like-RNase2* in all four accessions (Figure S2E), indicating that the abundance variation of S-like-RNase2 is not a result of gene deletion. Furthermore, we compared the sequences of the predicted promoter (~1,200 bp) and open reading frame (ORF) of *S-like-RNase* alleles among the four accessions. No SNP was found in the predicted promoter and one SNP was found in the ORF of AZ and UT *S-like-RNase1*, which results in a difference in amino acid 126 (Figure S2B). At this position, both asparagine in UT and aspartic acid in AZ were found in known *S-* or *S-like-RNases* [27],

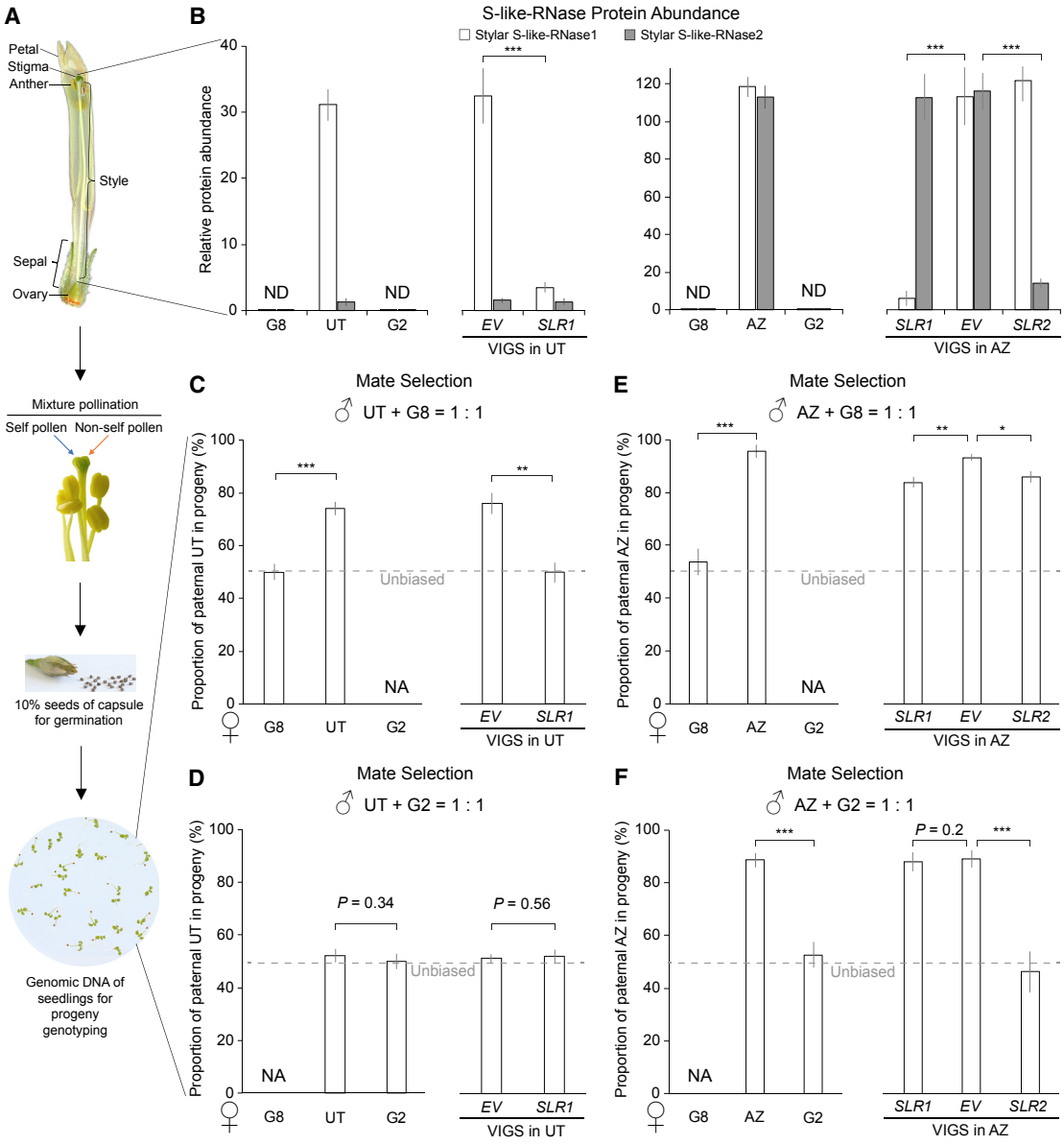

Figure 1. NaS-like-RNase1 and 2 Are Involved in Mate Selection

(A) Workflow schematic from stylar protein quantification, mixture pollinations with equal self and non-self pollen grains, and progeny paternity genotyping, conducted with 10% of the seeds of each mature capsule.

(B) Relative S-like-RNase1 and 2 protein abundance in the styles, expressed relative to *N. attenuata* elongation factor NaEF, of the indicated genotypes was quantified by LC-MS^E (mean ± SE, n = 3). Not detected, ND.

(C and D) The percentage seed siring by paternal UT genotype (mean ± SE, n = 4) was analyzed in capsules produced from emasculated flowers of the indicated maternal genotypes (♀) pollinated with (C) a 1:1 mixture of UT:G8 pollen (♂) or (D) a 1:1 mixture of UT:G2 pollen (♂).

(E and F) The percentage seed siring by paternal AZ genotype (mean ± SE, n = 4) was analyzed in capsules produced from emasculated flowers of the indicated maternal genotypes (♀) pollinated with (E) a 1:1 mixture of AZ:G8 pollen (♂) or (F) a 1:1 mixture of AZ:G2 pollen (♂).

For (C)–(F), each replicate represents a capsule resulting from an independent pollination. Asterisks indicate significant differences (*$p < 0.05$; **$p < 0.01$; ***$p < 0.001$; Student's t test); not analyzed, NA; *empty vector*, *EV*; *S-like-RNase1*, *SLR1*; *S-like-RNase2*, *SLR2*; the dotted line indicates unbiased seed set percentages for a 1:1 pollen mixture applied to the stigma.

See also Figure S1 and Tables S1 and S2.

suggesting that this SNP is not responsible for the abundance variation between UT and AZ. While we found a few SNPs in the *S-like-RNase2* of UT, the sequences are identical in G2, G8, and AZ (Figure S2E; Table S4). In summary, gene deletion and sequence mutations are not sufficient to explain the protein abundance variation of S-like-RNases.

In the SI almond, *Prunus dulcis*, DNA methylation is associated with S-RNase loss of function [28]. Hence, we analyzed DNA

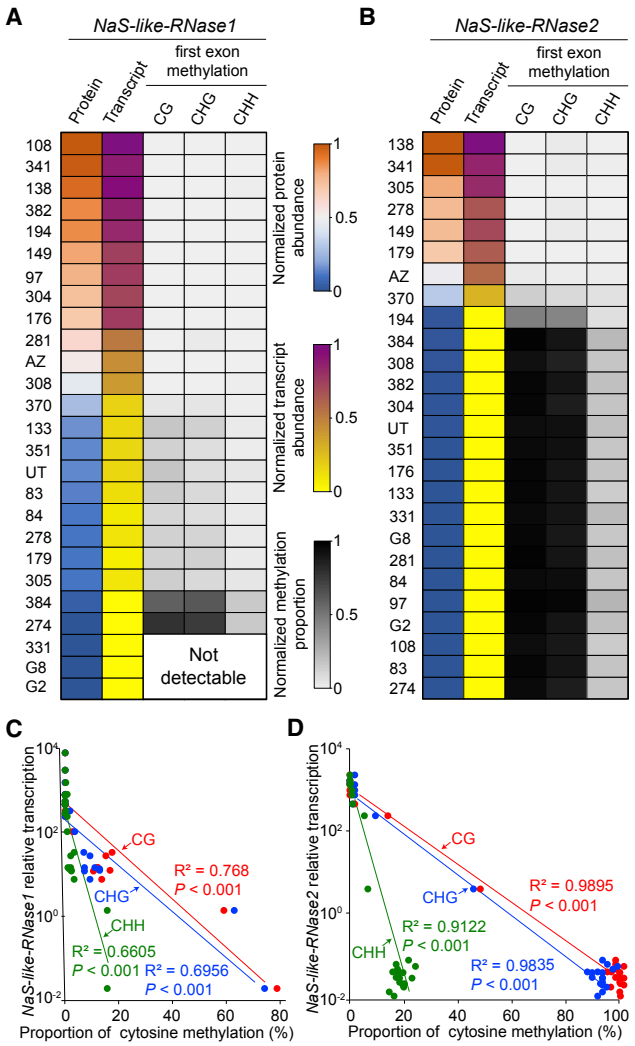

Figure 2. Natural Variation in NaS-like-RNase Abundance Is Highly Correlated with Coding Region Cytosine Methylation

(A and B) The normalized protein abundance (relative to NaEF and normalized as $X' = X/X_{max}$) and transcript abundance (relative to *NaEF* and normalized as $X' = X/X_{max}$) of (A) *NaS-like-RNase1* and (B) *NaS-like-RNase2*, and cytosine methylation rates (CG, CHG and CHH) in their first exon were quantified in 26 natural accessions of *N. attenuata*.

(C and D) Relative transcript abundance (relative to *NaEF*) is correlated with three different cytosine methylation rates in the first exon of (C) *NaS-like-RNase1* and (D) *NaS-like-RNase2*.

See also Figure S2 and Tables S1, S2, S4, S5, and S6.

methylations of cytosine-dense regions located in the predicted promoter and first exon of *S-like-RNase1* and *2*. Two neighboring cytosine-dense regions of *S-like-RNase1* showed significant differences in cytosine methylations between UT and AZ (Figure S2C; Table S5). Furthermore, four cytosine-dense regions of *S-like-RNase2* showed significant differences in cytosine methylation between AZ and other accessions (Figure S2F; Table S5). To investigate if these associations are widespread in natural populations, we compared the normalized protein and transcript abundances of *S-like-RNases* with the corresponding DNA methylation rates of their first exon in 22 additional natural accessions (26 in total) (Figures 2A and 2B; Table S6). In the natural accessions, relative transcript abundances of *S-like-RNase1* and *2* were strongly correlated with the rates of cytosine methylation (Figures 2C and 2D), suggesting that DNA methylation might be responsible for the protein abundance variation of *S-like-RNases*.

Pollen NaSLF-like Proteins Show Coordinated Expression and Direct Interactions with Stylar NaS-like-RNases

In solanaceous SI, the molecular interaction between male (SLF protein) and female (S-RNase) follows a collaborative non-self-recognition pattern, and ubiquitination of the S-RNase through an SCF^{SLF} (SSK1, CUL1, and F-box) complex provides a likely mechanism of S-RNase detoxification [14–18]. To determine if the mate selection of *N. attenuata* also results from multiple NaSLF-like proteins and the canonical collaborative recognition system, a genome-wide analysis identified one *SSK1*, one *CUL1*, and 14 *SLF-like* genes in both UT and AZ genomes. Premature stop codons were found in the coding sequences of eight *SLF-like* genes, which resulted in significantly smaller truncated proteins (54–186 amino acids) compared with the regular full-length SLF (~390 amino acids). No premature stop codon was found in the other six genes (*NaSLF-like1–6*), indicating that they are functional. All functional genes are specifically expressed in anthers and are homologous to the genes of cross-pollen compatibility in SI species (Figures S3A–S3D). Similar to the transcription pattern reported from SI *Petunia inflata* [29], we found a large variation in transcript abundances of *NaSLF-like1–6* compared with those of *NaSSK1* and *NaCUL1* (Figure S3F).

While the transcript abundances of *NaSLF-like1* and *6* were significantly correlated with *S-like-RNase2* transcript abundance, *NaSLF-like2* and *4* were significantly correlated with *S-like-RNase1* (Figures 3A and S3G–S3K). Furthermore, yeast-two-hybrid (Y2H) assays revealed that the C terminus of SLF-like1 directly interacts with S-like-RNase2, but not with S-like-RNase1 (Figure 3B), which corresponds to the coordinated expression of *SLF-like1* and *S-like-RNase2* in the 26 natural accessions. Similarly, SLF-like2 and 4 showed protein-protein interactions in Y2H assays with S-like-RNase1 (Figure S3L), which also corresponds to the correlated transcript abundances of these genes (Figures S3G and S3I). Moreover, we found PhSSK1, which is required for cross-pollen compatibility in SI *Petunia hybrida* [14], and NaSSK1 to interact with the N terminus of NaSLF-like1 (1–60 amino acids, thought to be the F-box domain) and NaCUL1 (Figure S3E), suggesting that NaSLF-like1 can interact with NaS-like-RNase2 by forming a canonical $SCF^{SLF\text{-}like1}$ complex.

Pollen SLF-like Genes Are Involved in Mate Selection

To determine if the interaction between SLF-like1 and S-like-RNase2 is involved in mate selection, *SLF-like1* was specifically silenced by VIGS (Figures 3C and S3M), and we pollinated emasculated flowers of AZ plants with equal pollen mixtures of G2 and either EV control (VIGS-*EV*/AZ) or *SLF-like1*-silenced lines (VIGS-*SLFL1*/AZ). Compared to G2:VIGS-*EV*/AZ pollen, a significant reduction of self-preference was found in the emasculated flowers of AZ plants pollinated with G2:VIGS-*SLFL1*/AZ pollen (Figure 3C). Moreover, to determine if the interactions between SLF-like2 or 4

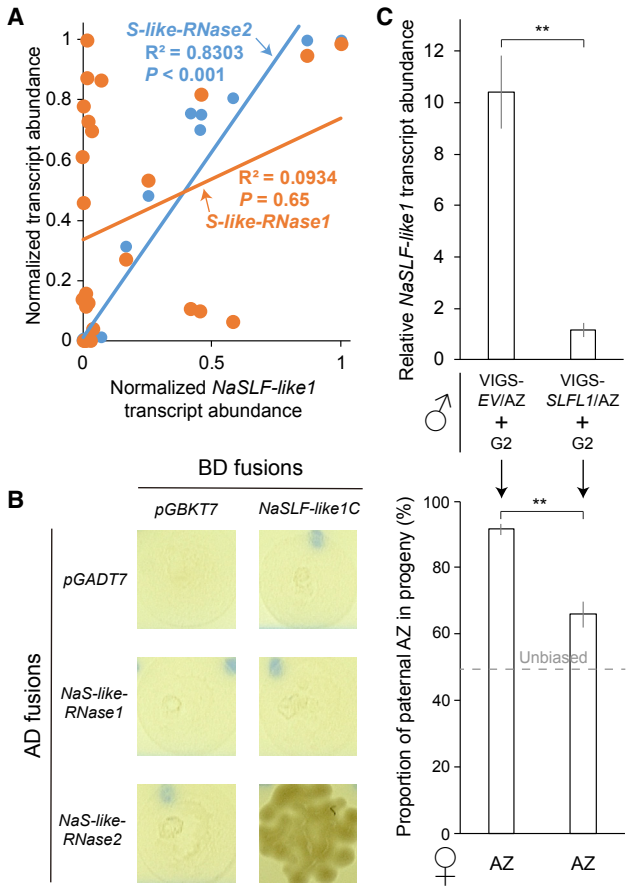

Figure 3. Pollen NaSLF-like1 Interacts Directly with Stylar NaS-like-RNase2 and Is Involved in Mate Selection

(A) Normalized transcript abundance (relative to *NaEF* and normalized as $X' = X/X_{max}$) of *NaSLF-like1* is strongly correlated with *NaS-like-RNase2* (blue) in 26 natural accessions, but not *NaS-like-RNase1* (orange).

(B) Yeast cells expressing different combinations of *NaSLF-like1C* (encoding C terminus without 1–60 amino acids) fused with BD and *S-like-RNases* fused with AD were tested for growth on -Leu/-Trp/-His/-Ade dropout media. Empty vector *pGBKT7* and *pGADT7* were used as negative controls.

(C) *NaSLF-like1* relative transcript abundance (top panel, mean ± SE, n = 4, relative to *NaEF*) was quantified in pollen of empty vector (VIGS-*EV*/AZ) and *SLF-like1*-silenced (VIGS-*SLFL1*/AZ) AZ transgenic lines. The percentage seed siring by paternal AZ genotype (bottom panel, mean ± SE, n = 4) was determined in progeny of mixed pollinations. Emasculated flowers of AZ plants were pollinated with equal pollen mixtures from G2 and either VIGS-*EV*/AZ or VIGS-*SLFL1*/AZ plants, respectively. Each replicate represents a capsule resulting from an independent pollination. Asterisks indicate significant differences (*p < 0.05; **p < 0.01; ***p < 0.001; Student's t test); the dotted line indicates unbiased seed set percentage for a 1:1 pollen mixture applied to the stigma.

See also Figures S1 and S3 and Table S2.

and S-like-RNase1 are involved in mate selection, *SLF-like2* or *4* or *SLF-like2* and *4* together, respectively, were specifically silenced by VIGS (Figure S3O). The emasculated flowers of UT plants were pollinated with equal pollen mixtures of G8 and EV control (VIGS-*EV*/AZ) or *SLF-like2*-silenced lines (VIGS-*SLFL2*/UT), *SLF-like4*-silenced lines (VIGS-*SLFL4*/UT), or *SLF-like2* and *4*-dually silenced lines (VIGS-*SLFL2&4*/UT). Compared to VIGS-*EV*/UT pollen, a significant reduction of self-preference was found in emasculated UT flowers pollinated with either G8:VIGS-*SLFL2*/UT or G8:VIGS-*SLFL2&4*/UT pollen, respectively (Figure S3N). Silencing *SLF-like4* alone had a weaker effect on mate selection, and the reduction in self-preference compared with VIGS-*EV*/*UT* was not statistically significant. SLF-like 2 and 4 contributed to G8 pollen discrimination by UT styles in an additive manner (Figure S3N). Together, these results demonstrate that both pollen-expressed NaSLF-like proteins and style-expressed NaS-like-RNase are involved in mate selection in *N. attenuata*.

Flowers Select Mates from Plants with Similar S-like-RNase Expression Patterns

Based on the coordinated expression and direct interactions between specific NaS-like-RNase and SLF-like proteins and their involvement in mate selection, we predict that styles expressing S-like-RNases would select mates from plants with corresponding S-like-RNase expression patterns. To test this hypothesis, an RNAi construct containing a DNA fragment of *S-like-RNase1* in an inverted-repeat orientation was transformed into UT (ir*SLR1*/UT), and a similar construct for silencing *S-like-RNase2* was transformed into AZ (ir*SLR2*/AZ). Independent transgenic lines in the T_2 generation, each homozygous for a single transgene insertion with diminished protein abundance of S-like-RNase1 (~98.9%) in UT or S-like-RNase2 (~97.8%) in AZ (Figure S4; Table S1), were used for all experiments. We selected 14 of the 26 accessions as pollen donors based on their S-RNase-like expression profiles (Figures 2A and 2B; Table S1). Three accessions (274, 331, and 384) express small amounts of both S-like-RNase1 and 2, similar to the pattern observed in ir*SLR1*/UT. Six accessions (97, 108, 133, 194, 281, and 351) express S-like-RNase1, but not S-like-RNase2, similar to wild-type and EV/UT and ir*SLR2*/AZ, and five accessions (138, 278, 305, 341, and 370) express both S-like-RNase1 and 2, similar to the pattern observed in wild-type and EV/AZ (Figure 4A). Equal amounts of pollen grains from all 14 accessions were mixed to pollinate the emasculated flowers of five genotypes: G2, *EV*/UT, ir*SLR1*/UT, *EV*/AZ, and ir*SLR2*/AZ. A suite of three microsatellite markers was developed to distinguish the paternity of seeds sired by the 14 pollen donors (Tables S2 and S6; STAR Methods).

We used emasculated flowers of an ethylene-deficient UT line, silenced in the expression of 1-aminocyclopropane-1-carboxylic acid oxidase (ir*ACO*/UT), which have a completely abolished mate selection phenotype [26], to determine the seed siring capacity of the 14 paternal genotypes in the mixture (Figures S4E and S4F). The results of the progeny paternity analysis from ir*ACO*/UT indicate that pollen grains from all 14 genotypes were equally capable in siring seeds and sired relatively similar numbers of seeds from the mixed-genotype pollen loads (Figure S4F, bottom panel). Emasculated flowers of G2 plants, which completely lacked stylar expression of both S-like-RNase1 and 2 (Figure 1B; Table S1), showed no significant difference among seed paternal genotypes compared to the non-selective ir*ACO*/UT plants pollinated with the 14 equal pollen grain mixtures (Figure S4F), indicating that G2 flowers had also lost the capability of mate selection. Compared to G2 flowers, emasculated flowers of *EV*/UT plants, which express only S-like-RNase1 (Table S1), discriminated against pollen from two accessions

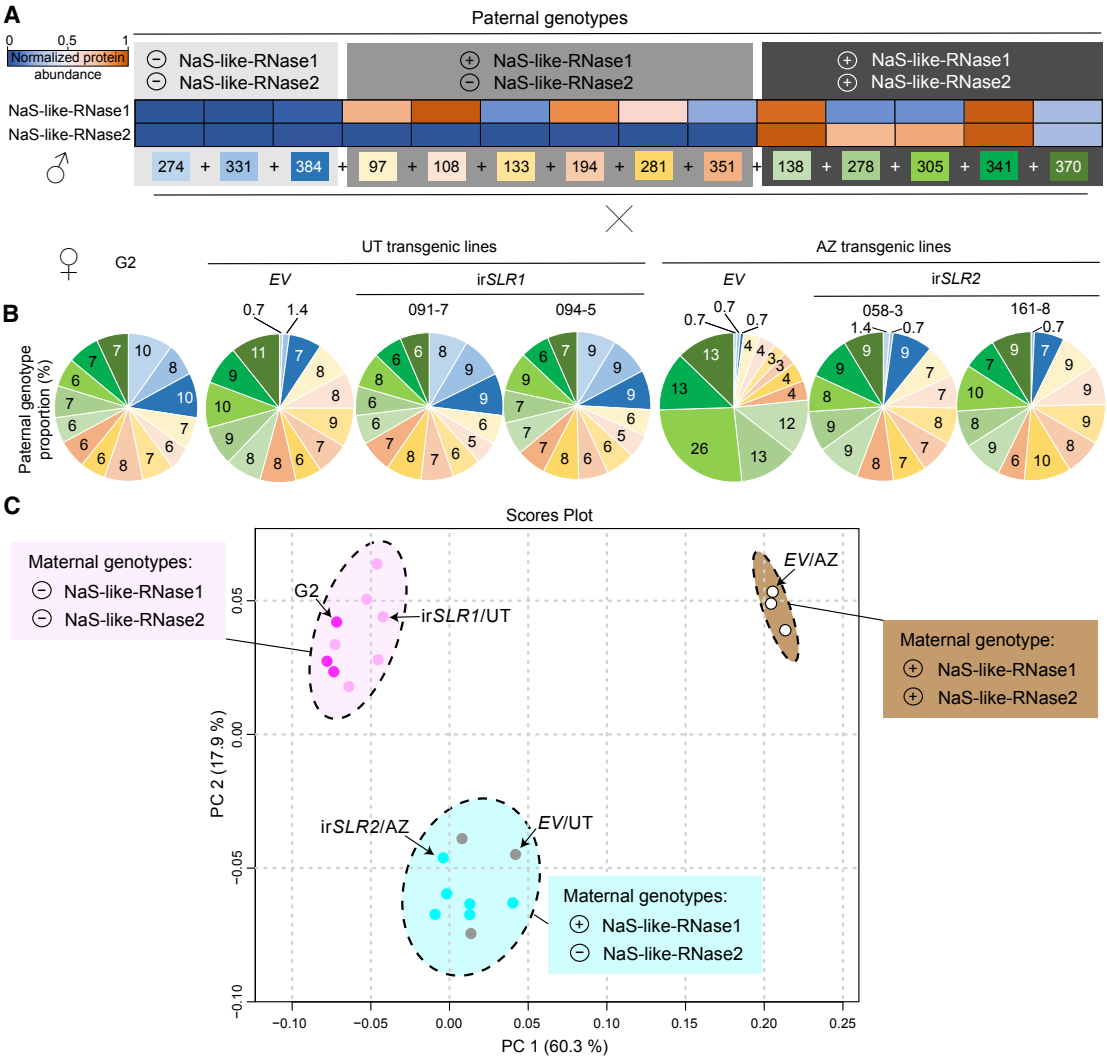

Figure 4. Styles Select Pollen from Plants with Similar S-like-RNase Expression Patterns

(A) Heatmap of normalized protein abundance (relative to NaEF and normalized as $X' = X/X_{max}$) of NaS-like-RNase1 and 2. Protein abundances were quantified in styles of 14 pollen donors (♂), from which the pollen was mixed in equal ratios to conduct mixture pollinations. Emasculated flowers of the following maternal genotypes (♀) were pollinated with the equal non-self pollen mixtures: wild-type G2, *S-like-RNase1* silenced in UT (ir*SLR1*/UT), *S-like-RNase2* silenced in AZ (ir*SLR2*/AZ), and the empty vector (*EV*/UT and *EV*/AZ) transgenic control lines.

(B) Pie charts of the percentage (mean of three replicates; each replicate represents a capsule resulting from an independent pollination) of paternal genotypes of seeds fertilized by the mixture pollinations. Slice colors correspond to the colors shown in (A). From each capsule, at least 50 seeds were germinated. Genomic DNA was extracted from the 2-week-old seedlings and analyzed for paternity by three microsatellite markers optimized to genotype these particular *N. attenuata* accessions.

(C) Principal component analysis (PCA) score plot constructed from the paternity percentages reported in (B). Dots in different colors indicate maternal genotypes. The ellipses indicate three different S-like-RNase expression patterns.

See also Figure S4 and Tables S1, S2, and S6.

(274 and 331; Figure 4B), which lack expression of both S-like-RNase1 and 2 (Figure 4A; Table S1). Silencing of S-RNase-like1 in UT abolished this mate selection and flowers from *irSLR1*/UT plants produced progeny with the same genotype distributions as flowers from the non-selective G2 and *irACO*/UT plants. Styles of *EV*/AZ, which express both S-like-RNase1 and 2, selected pollen from five accessions (Figure 4B), all of which displayed similar expression patterns of S-like-RNases as does *EV*/AZ (Figure 4A; Table S1).

A principal component analysis revealed that seeds produced from G2 and ir*SLR1*/UT displayed similar progeny paternity distributions and thus were clustered into one group, which is consistent with the lack of expression of both S-like-RNase1 and 2 in their styles. Seeds produced by *EV*/UT and ir*SLR2*/AZ displayed similar progeny paternity distribution and, therefore, were clustered into a separate group, which is consistent with the expression of only S-like-RNase1 in their styles. Progeny paternity of seeds from replicate *EV*/AZ were clustered into a third

group. Taken together, these results are fully consistent with the hypothesis that flowers select mates from plants with similar S-like-RNase expression patterns.

DISCUSSION

Flowering plants with different mating systems have evolved multiple patterns of intraspecific mate preference. The S-RNase-based SI system found in obligate outbreeding solanaceous populations is one of the best studied intraspecific pollen rejection mechanisms [19]. In addition, SI homologous genes may be involved in another type of intraspecific pollen rejection, the intraspecific UI system [20, 21], indicating the potential link and complexity among different patterns of intraspecific mate preference. In contrast to the SI and intraspecific UI, a polyandrous mate selection was identified in the SC *N. attenuata* [26]. However, the underlying molecular mechanism has not been characterized and the results reported here revealed that NaS-like-RNases are involved in mate selection by exerting an unknown effect on the fertilization preference of particular pollen genotypes in mixture pollinations. The allelic variation in DNA methylation of *NaS-like-RNases* is significantly correlated to their transcript abundance in 26 natural accessions of the SC *N. attenuata*. We identified coordinated expression patterns between S-like-RNases and SLF-like proteins among the 26 natural accessions. Utilizing natural variation in the expression of S-like-RNases and SLF-like proteins in combination with targeted RNAi-based manipulations, we show the S-RNase-SLF recognition mechanism plays a central role in the polyandrous mate selection in the SC *N. attenuata*.

In the classical S-RNase-based SI system, *S-RNase* and multiple *SLF* genes are tightly linked to the *S*-locus [8, 11, 30], which is crucial for the suppression of recombination among different *S*-haplotypes and the stability of SI in obligate outbreeding populations [19]. Interestingly, particular combinations of *NaS-like-RNases* and *NaSLF-like* genes with coordinated transcript abundances and the ability to directly interact in Y2H assays were demonstrated to be functional in the mate selection in the fully SC *N. attenuata* (Figures 3 and S3), implying that *S-like-RNase* might be linked to their corresponding *SLF-like* genes. A preliminary analysis of the *N. attenuata* genome suggests that the assembled scaffolds containing *S-like-RNases* and *SLF-like* genes might be tightly linked to each other based on the synteny of the predicted *S*-locus on chromosome 1 of *Solanum lycopersicum* Heinz (https://solgenomics.net). However, no overlapping regions among any pair of scaffolds were found. According to the length of the predicted *S*-locus in SC *Antirrhinum majus* L. (length of the *S*-locus: ~0.87 Mb and genome size: ~0.52 Gb), *Petunia axillaris* (length of the *S*-locus: ~8.0 Mb and genome size: ~1.4 Gb), *Petunia inflata* (length of the *S*-locus: ~11.3 Mb and genome size: ~1.4 Gb), *Solanum tuberosum L.* (length of the *S*-locus: ~17.9 Mb and genome size ~0.84 Gb), and *Solanum lycopersicum* (length of the *S*-locus: ~14.5 Mb and genome size ~0.9 Gb) [18, 31–34], the size of the predicted *S*-locus in SC *N. attenuata* appears to be substantially larger (genome size of *N. attenuata*: ~2.5 Gb) [35] and the linkage relationships of *S-like-RNases* and *SLF-like* genes remain unclear. Further experiments, i.e., chromosome fluorescence *in situ* hybridization (FISH) and a higher quality genome assembly, are needed to assess the linkage relationship between *S-like-RNases* and their corresponding *SLF-like* genes.

A previous study clearly demonstrated that differences in competitive ability of pollen tubes, rather than pollen tube acceptance, were associated with mate selection in the SC *N. attenuata* [26]. Comparisons of mate selection between control and *S-like-RNase*-silenced lines revealed that S-like-RNases are required for mate selection (Figures 1 and 4). Taken together, these results imply that the role of NaS-like-RNases in mate selection is different from their cytotoxic mode of action suggested in the classical SI response [4–7]. However, it is not clear how S-like-RNases lead to the mate selection in *N. attenuata*. The results presented here are consistent with two mechanistic hypotheses: (1) in the absence of interacting SLF-like proteins, S-like-RNases have a detrimental effect on the growth of unfavored pollen tubes or (2) interactions between particular S-like-RNases and SLF-like proteins promote or protect the growth of favored pollen tubes. To discern the mechanism underlying mate selection in *N. attenuata*, further experiments are needed to compare the growth rates of SLF-like expressing and deficient pollen tubes in styles with and without expression of specific S-like-RNases. Table S7 shows the predicted outcome of pollen tube growth assays, which could distinguish between the mechanisms involving S-like-RNases as detrimental factors on unfavored pollen tubes or SLR-SLFL interactions promoting or protecting the growth of favored pollen tubes (Figure 5).

The activity of S-RNase is dependent on multiple aspects: specific ribonuclease activity, expression abundance, particular temporal and spatial expression profile, subcellular localization, and interactions with its modifiers [36–40], all of which should be evaluated in NaS-like-RNases. The complete abrogation of mate selection in the ethylene-deficient lines [26] and the *NaS-like-RNase1/2*-deficient G2 natural accession begs the question if and how the post-pollination ethylene burst [26] influences stylar *NaS-like-RNase* expression and activity. This is will be a central objective of future work into this system.

Despite a few cases of gene deletions of *NaS-like-RNase1* (Figure S2A), the strong correlation between the variation in transcript abundances of *S-like-RNases* and the cytosine methylation rates of their first exon that was observed in *N. attenuata* natural accessions (Figures S2C, S2F, and 2) is highly consistent with the association between methylation of the S_f locus and loss of function of S-RNase in SC *Prunus dulcis* [28]. To examine if DNA methylation results in the observed variation in S-like-RNase abundance and the corresponding mate selection, targeted DNA demethylation assays [41] followed by S-like-RNase protein quantification and mate selection analysis are needed. Alternatively, the *trans*-acting element (e.g., particular small RNAs) controlling the cytosine methylation of *S-like-RNase* genes could be identified and manipulated.

The SI-SC transition has been considered one of the most frequent evolutionary transitions in flowering plants [24, 42], which is thought to be strongly selected for in small, fragmented populations where finding non-self mates can severely limit the fitness of SI plants. The lack of any apparent inbreeding depression after more than 20 consecutive generations of selfing in UT and AZ (30 and 21 generations of selfing, respectively) [22] is consistent with the inference that recessive deleterious mutations have either been purged or fixed during population bottlenecks in the long

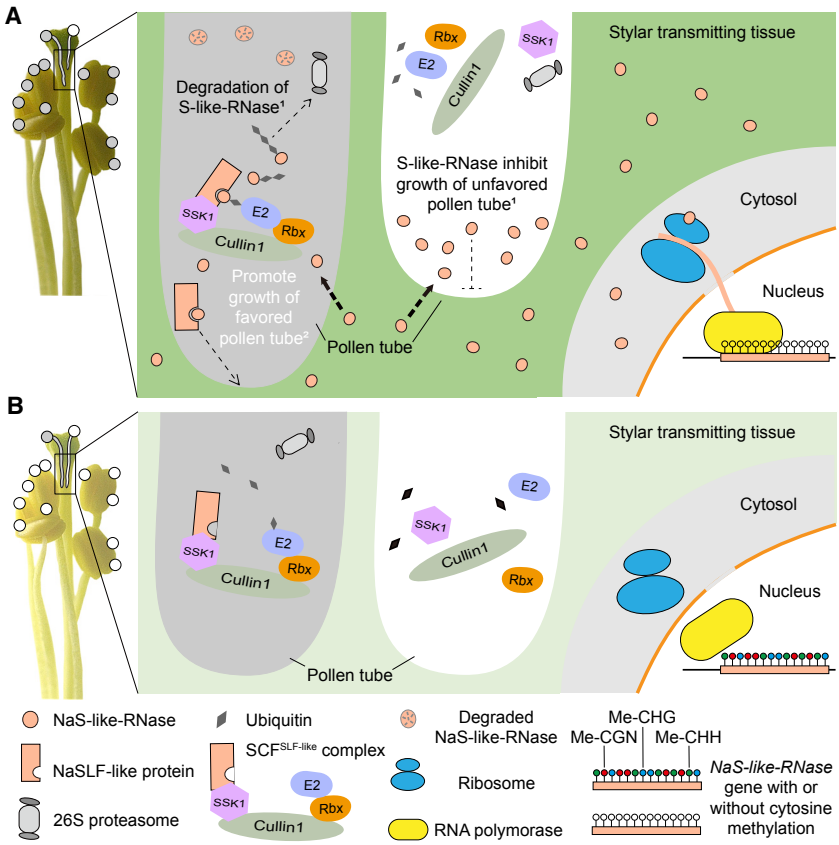

Figure 5. Schematic of Two Proposed S-like-RNase-Mediated Mechanisms Underlying Mate Selection in SC *N. attenuata*

(A) Mate selection is observed in mixture pollinations in styles with expression of NaS-like-RNase(s). After penetrating into both favored and unfavored pollen tubes from the stylar transmitting tissue, S-like-RNase could interact with their corresponding SLF-like proteins in the favored pollen tubes. One hypothesis[1] is that the interaction between S-like-RNase and $SCF^{SLF\text{-}like}$ in favored pollen tubes results in the degradation of S-like-RNase via the ubiquitination-26S proteasome pathway, while in the unfavored pollen tube, lacking the expression of the corresponding SLF-like protein, S-like-RNase has a detrimental effect on growth of pollen tubes, leading to mate selection. An alternative hypothesis[2] is that interactions between S-like-RNase and SLF-like proteins promote or protect the growth of favored pollen tubes through an unknown mechanism.

(B) Styles lacking the expression of S-like-RNase do not discriminate pollen in mixture pollinations.

See also Table S7.

history of selfing in *N. attenuata* [42]. This lack of inbreeding depression is also consistent with the phylogenetic inference that the SI-SC transition occurred in the ancestral species of *N. attenuata* ~10.8 million years ago (Figure S1A) [24, 25]. Although self-fertilization is predominant in *N. attenuata* [22] and genetic diversity is predicted to decrease as a result of autogamy, it is surprising that natural *N. attenuata* populations have been shown to harbor substantial genetic diversity [43]. We hypothesize that this genetic diversity results in part from the smoke-synchronized germination of dormant seeds of different ages that were deposited in the long-lived (more than 150 years) seed banks at very different times [44–47]. In the equal pollen load mixture pollinations with 14 non-self pollen donors, which were previously shown to harbor considerable genetic and metabolic diversity [48], flowers expressing particular NaS-like-RNases selected mates from accessions with corresponding expression patterns of S-like-RNases (Figure 4), indicating that *N. attenuata* plants expressing S-like-RNase(s) select particular mates among genotypes of non-self pollen, and the self pollen preference (Figures 1C, 1E, and 1F) might be a by-product as a result of ancient SI-SC transition. Therefore, we hypothesize that when pollen loads with genetically diverse pollen grains are delivered to stigmas by pollinators, the mate selection mechanisms described here could select particular mates with beneficial trait(s) that link to certain expression patterns of S-like-RNase(s). We presume that plants that produce seeds with beneficial trait(s) will have a greater number of offspring that survive the long wait in the seed bank until the next fire synchronizes their germination. In summary, we suppose that ecological factors, such as fire-disturbance regimes, which decrease a species' effective population sizes, selected for the SI-SC transition in ancestral *N. attenuata* populations. Once the transition to SC had purged deleterious mutations, the SI machinery could be repurposed as a mate selection tool, perhaps to transfer beneficial trait(s) to their offspring. However, an alternative hypothesis is that in *N. attenuata*, the remnant of an SI system has become non-functional and its machinery is gradually being pseudogenized. For instance, accessions with NaS-like-RNases expression (e.g., UT and AZ) might be in a transitional stage with reduced fitness compared to other accessions with a complete loss of expression of NaS-like-RNases (e.g., G2 and G8). This hypothesis requires further testing by comparing the survival rates of seeds sired by selective and non-selective accessions in native seed banks and their fitness in native habitats. Whether the mate selection mechanisms described here allow plants to make adaptive mate choices and sire seeds with specific traits that increase seed/seedling survival is an intriguing question that will require many additional decades of research. However, now that the mate selection mechanisms are understood, it is possible to test this hypothesis. With the tools available to manipulate the mate selection mechanisms that plants use, it should be possible to create genetically comparable seed banks sired from selected and non-selected mates.

STAR★METHODS

Detailed methods are provided in the online version of this paper and include the following:

- KEY RESOURCES TABLE
- CONTACT FOR REAGENT AND RESOURCE SHARING

SUPPLEMENTAL INFORMATION

Supplemental Information can be found online at https://doi.org/10.1016/j.cub.2019.05.042.

ACKNOWLEDGMENTS

We thank the glasshouse team of the Max Planck Institute for Chemical Ecology for plant cultivation; Dapeng Li, Wenwu Zhou, Jiancai Li, Aleš Svatoš, Yvonne Hupfer, Domenica Schnabelrauch, and Eva Rothe for technical assistance; and Boris Igić, Lei Hou, and Shuqing Xu for fruitful discussions. This work was supported by the Max Planck Society and Advanced Grant no. 293926 of the European Research Council to I.T.B.

AUTHOR CONTRIBUTIONS

H.G., R.H., and I.T.B. designed research; H.G., N.W., and K.G. performed research; I.T.B. contributed new reagents and analytic tools; H.G., R.H., N.W., and I.T.B. analyzed data; and H.G., R.H., and I.T.B. wrote the paper. All authors revised the manuscript.

DECLARATION OF INTERESTS

The authors declare no conflicts of interest.

Received: February 27, 2019
Revised: April 16, 2019
Accepted: May 17, 2019
Published: June 6, 2019

REFERENCES

1. De Nettancourt, D. (1997). Incompatibility in angiosperms. Sex. Plant Reprod. *10*, 185–199.
2. De Nettancourt, D. (2001). Incompatibility and Incongruity in Wild and Cultivated Plants (Springer Verlag GmbH).
3. Takayama, S., and Isogai, A. (2005). Self-incompatibility in plants. Annu. Rev. Plant Biol. *56*, 467–489.
4. Anderson, M.A., Cornish, E.C., Mau, S.L., Williams, E.G., Hoggart, R., Atkinson, A., Bonig, I., Grego, B., Simpson, R., Roche, P.J., et al. (1986). Cloning of cDNA for a stylar glycoprotein associated with expression of self-incompatibility in *Nicotiana alata*. Nature *321*, 38.
5. Kowyama, Y., Kunz, C., Lewis, I., Newbigin, E., Clarke, A.E., and Anderson, M.A. (1994). Self-compatibility in a*Lycopersicon peruvianum* variant (LA2157) is associated with a lack of style S-RNase activity. Theor. Appl. Genet. *88*, 859–864.
6. Lee, H.-S., Huang, S., and Kao, T. (1994). S proteins control rejection of incompatible pollen in *Petunia inflata*. Nature *367*, 560–563.
7. McClure, B.A., Haring, V., Ebert, P.R., Anderson, M.A., Simpson, R.J., Sakiyama, F., and Clarke, A.E. (1989). Style self-incompatibility gene products of Nicotiana alata are ribonucleases. Nature *342*, 955–957.
8. Lai, Z., Ma, W., Han, B., Liang, L., Zhang, Y., Hong, G., and Xue, Y. (2002). An F-box gene linked to the self-incompatibility (*S*) locus of *Antirrhinum* is expressed specifically in pollen and tapetum. Plant Mol. Biol. *50*, 29–42.
9. Qiao, H., Wang, F., Zhao, L., Zhou, J., Lai, Z., Zhang, Y., Robbins, T.P., and Xue, Y. (2004). The F-box protein AhSLF-S_2 controls the pollen function of S-RNase-based self-incompatibility. Plant Cell *16*, 2307–2322.
10. Qiao, H., Wang, H., Zhao, L., Zhou, J., Huang, J., Zhang, Y., and Xue, Y. (2004). The F-box protein AhSLF-S_2 physically interacts with S-RNases that may be inhibited by the ubiquitin/26S proteasome pathway of protein degradation during compatible pollination in *Antirrhinum*. Plant Cell *16*, 582–595.
11. Sijacic, P., Wang, X., Skirpan, A.L., Wang, Y., Dowd, P.E., McCubbin, A.G., Huang, S., and Kao, T.H. (2004). Identification of the pollen determinant of S-RNase-mediated self-incompatibility. Nature *429*, 302–305.
12. Zhang, Y., Zhao, Z., and Xue, Y. (2009). Roles of proteolysis in plant self-incompatibility. Annu. Rev. Plant Biol. *60*, 21–42.
13. Huang, J., Zhao, L., Yang, Q., and Xue, Y. (2006). AhSSK1, a novel SKP1-like protein that interacts with the *S*-locus F-box protein SLF. Plant J. *46*, 780–793.
14. Zhao, L., Huang, J., Zhao, Z., Li, Q., Sims, T.L., and Xue, Y. (2010). The Skp1-like protein SSK1 is required for cross-pollen compatibility in *S*-RNase-based self-incompatibility. Plant J. *62*, 52–63.
15. Li, W., and Chetelat, R.T. (2014). The role of a pollen-expressed Cullin1 protein in gametophytic self-incompatibility in *Solanum*. Genetics *196*, 439–442.
16. Kubo, K.I., Tsukahara, M., Fujii, S., Murase, K., Wada, Y., Entani, T., Iwano, M., and Takayama, S. (2016). Cullin1-P is an essential component of non-self recognition system in self-incompatibility in *Petunia*. Plant Cell Physiol. *57*, 2403–2416.
17. Kubo, K., Entani, T., Takara, A., Wang, N., Fields, A.M., Hua, Z., Toyoda, M., Kawashima, S., Ando, T., Isogai, A., et al. (2010). Collaborative non-self recognition system in S-RNase-based self-incompatibility. Science *330*, 796–799.
18. Kubo, K., Paape, T., Hatakeyama, M., Entani, T., Takara, A., Kajihara, K., Tsukahara, M., Shimizu-Inatsugi, R., Shimizu, K.K., and Takayama, S. (2015). Gene duplication and genetic exchange drive the evolution of S-RNase-based self-incompatibility in *Petunia*. Nat. Plants *1*, 14005.
19. Fujii, S., Kubo, K., and Takayama, S. (2016). Non-self- and self-recognition models in plant self-incompatibility. Nat. Plants *2*, 16130.
20. Broz, A.K., Randle, A.M., Sianta, S.A., Tovar-Méndez, A., McClure, B., and Bedinger, P.A. (2017). Mating system transitions in *Solanum habrochaites* impact interactions between populations and species. New Phytol. *213*, 440–454.
21. Bedinger, P.A., Chetelat, R.T., McClure, B., Moyle, L.C., Rose, J.K., Stack, S.M., van der Knaap, E., Baek, Y.S., Lopez-Casado, G., Covey, P.A., et al. (2011). Interspecific reproductive barriers in the tomato clade: opportunities to decipher mechanisms of reproductive isolation. Sex. Plant Reprod. *24*, 171–187.
22. Sime, K.R., and Baldwin, I.T. (2003). Opportunistic out-crossing in *Nicotiana attenuata* (Solanaceae), a predominantly self-fertilizing native tobacco. BMC Ecol. *3*, 6.
23. Kessler, D., Gase, K., and Baldwin, I.T. (2008). Field experiments with transformed plants reveal the sense of floral scents. Science *321*, 1200–1202.

24. Goldberg, E.E., Kohn, J.R., Lande, R., Robertson, K.A., Smith, S.A., and Igić, B. (2010). Species selection maintains self-incompatibility. Science *330*, 493–495.

25. Robertson, K., Goldberg, E.E., and Igić, B. (2011). Comparative evidence for the correlated evolution of polyploidy and self-compatibility in Solanaceae. Evolution *65*, 139–155.

26. Bhattacharya, S., and Baldwin, I.T. (2012). The post-pollination ethylene burst and the continuation of floral advertisement are harbingers of non-random mate selection in *Nicotiana attenuata*. Plant J. *71*, 587–601.

27. Xue, Y., Carpenter, R., Dickinson, H.G., and Coen, E.S. (1996). Origin of allelic diversity in *antirrhinum S* locus RNases. Plant Cell *8*, 805–814.

28. Fernández i Martí, A., Gradziel, T.M., and Socias i Company, R. (2014). Methylation of the S_f locus in almond is associated with *S*-RNase loss of function. Plant Mol. Biol. *86*, 681–689.

29. Williams, J.S., Der, J.P., dePamphilis, C.W., and Kao, T.H. (2014). Transcriptome analysis reveals the same 17 *S-locus F-box* genes in two haplotypes of the self-incompatibility locus of *Petunia inflata*. Plant Cell *26*, 2873–2888.

30. Li, J.-H., Nass, N., Kusaba, M., Dodds, P.N., Treloar, N., Clarke, A.E., and Newbigin, E. (2000). A genetic map of the *Nicotiana alata S*-locus that includes three pollen-expressed genes. Theor. Appl. Genet. *100*, 956–964.

31. Li, M., Zhang, D., Gao, Q., Luo, Y., Zhang, H., Ma, B., Chen, C., Whibley, A., Zhang, Y., Cao, Y., et al. (2019). Genome structure and evolution of *Antirrhinum majus* L. Nat. Plants *5*, 174–183.

32. Li, W., and Chetelat, R.T. (2015). Unilateral incompatibility gene *ui1.1* encodes an *S*-locus F-box protein expressed in pollen of *Solanum* species. Proc. Natl. Acad. Sci. USA *112*, 4417–4422.

33. Bombarely, A., Moser, M., Amrad, A., Bao, M., Bapaume, L., Barry, C.S., Bliek, M., Boersma, M.R., Borghi, L., Bruggmann, R., et al. (2016). Insight into the evolution of the Solanaceae from the parental genomes of *Petunia hybrida*. Nat. Plants *2*, 16074.

34. Xu, X., Pan, S., Cheng, S., Zhang, B., Mu, D., Ni, P., Zhang, G., Yang, S., Li, R., Wang, J., et al.; Potato Genome Sequencing Consortium (2011). Genome sequence and analysis of the tuber crop potato. Nature *475*, 189–195.

35. Xu, S., Brockmöller, T., Navarro-Quezada, A., Kuhl, H., Gase, K., Ling, Z., Zhou, W., Kreitzer, C., Stanke, M., Tang, H., et al. (2017). Wild tobacco genomes reveal the evolution of nicotine biosynthesis. Proc. Natl. Acad. Sci. USA *114*, 6133–6138.

36. Murfett, J., Strabala, T.J., Zurek, D.M., Mou, B., Beecher, B., and McClure, B.A. (1996). *S*-RNase and interspecific pollen rejection in the genus *Nicotiana*: multiple pollen-rejection pathways contribute to unilateral incompatibility between self-incompatible and self-compatible species. Plant Cell *8*, 943–958.

37. McClure, B., Mou, B., Canevascini, S., and Bernatzky, R. (1999). A small asparagine-rich protein required for *S*-allele-specific pollen rejection in *Nicotiana*. Proc. Natl. Acad. Sci. USA *96*, 13548–13553.

38. Hancock, C.N., Kent, L., and McClure, B.A. (2005). The stylar 120 kDa glycoprotein is required for *S*-specific pollen rejection in *Nicotiana*. Plant J. *43*, 716–723.

39. Goldraij, A., Kondo, K., Lee, C.B., Hancock, C.N., Sivaguru, M., Vazquez-Santana, S., Kim, S., Phillips, T.E., Cruz-Garcia, F., and McClure, B. (2006). Compartmentalization of S-RNase and HT-B degradation in self-incompatible *Nicotiana*. Nature *439*, 805–810.

40. Qin, X., Liu, B., Soulard, J., Morse, D., and Cappadocia, M. (2006). Style-by-style analysis of two sporadic self-compatible *Solanum chacoense* lines supports a primary role for S-RNases in determining pollen rejection thresholds. J. Exp. Bot. *57*, 2001–2013.

41. Gallego-Bartolomé, J., Gardiner, J., Liu, W., Papikian, A., Ghoshal, B., Kuo, H.Y., Zhao, J.M., Segal, D.J., and Jacobsen, S.E. (2018). Targeted DNA demethylation of the *Arabidopsis* genome using the human TET1 catalytic domain. Proc. Natl. Acad. Sci. USA *115*, E2125–E2134.

42. Shimizu, K.K., and Tsuchimatsu, T. (2015). Evolution of selfing: recurrent patterns in molecular adaptation. Annu. Rev. Ecol. Evol. Syst. *46*, 593–622.

43. Bahulikar, R.A., Stanculescu, D., Preston, C.A., and Baldwin, I.T. (2004). ISSR and AFLP analysis of the temporal and spatial population structure of the post-fire annual, *Nicotiana attenuata*, in SW Utah. BMC Ecol. *4*, 12.

44. Baldwin, I.T., Staszak-Kozinski, L., and Davidson, R. (1994). Up in smoke: I. Smoke-derived germination cues for postfire annual, *Nicotiana attenuata* torr. Ex. Watson. J. Chem. Ecol. *20*, 2345–2371.

45. Baldwin, I.T., and Morse, L. (1994). Up in smoke: II. Germination of *Nicotiana attenuata* in response to smoke-derived cues and nutrients in burned and unburned soils. J. Chem. Ecol. *20*, 2373–2391.

46. Preston, C.A., and Baldwin, I.T. (1999). Positive and negative signals regulate germination in the post-fire annual, *Nicotiana attenuata*. Ecology *80*, 481–494.

47. Wright, H.A., Neuenschwander, L.F., and Britton, C.M. (1979). The Role and Use of Fire in Sagebrush-Grass and Pinyon-Juniper Plant Communities: A State-of-the-Art Review (Intermountain Forest and Range Experiment Station, Forest Service, U.S. Department of Agriculture).

48. Li, D., Baldwin, I.T., and Gaquerel, E. (2015). Navigating natural variation in herbivory-induced secondary metabolism in coyote tobacco populations using MS/MS structural analysis. Proc. Natl. Acad. Sci. USA *112*, E4147–E4155.

49. Saedler, R., and Baldwin, I.T. (2004). Virus-induced gene silencing of jasmonate-induced direct defences, nicotine and trypsin proteinase-inhibitors in *Nicotiana attenuata*. J. Exp. Bot. *55*, 151–157.

50. Krügel, T., Lim, M., Gase, K., Halitschke, R., and Baldwin, I.T. (2002). *Agrobacterium*-mediated transformation of *Nicotiana attenuata*, a model ecological expression system. Chemoecology *12*, 177–183.

51. Bubner, B., Gase, K., Berger, B., Link, D., and Baldwin, I.T. (2006). Occurrence of tetraploidy in *Nicotiana attenuata* plants after *Agrobacterium*-mediated transformation is genotype specific but independent of polysomaty of explant tissue. Plant Cell Rep. *25*, 668–675.

52. von Dahl, C.C., Winz, R.A., Halitschke, R., Kühnemann, F., Gase, K., and Baldwin, I.T. (2007). Tuning the herbivore-induced ethylene burst: the role of transcript accumulation and ethylene perception in *Nicotiana attenuata*. Plant J. *51*, 293–307.

53. Kumar, S., Stecher, G., and Tamura, K. (2016). MEGA7: molecular evolutionary genetics analysis version 7.0 for bigger datasets. Mol. Biol. Evol. *33*, 1870–1874.

54. Henderson, I.R., Chan, S.R., Cao, X., Johnson, L., and Jacobsen, S.E. (2010). Accurate sodium bisulfite sequencing in plants. Epigenetics *5*, 47–49.

55. Hetzl, J., Foerster, A.M., Raidl, G., and Mittelsten Scheid, O. (2007). CyMATE: a new tool for methylation analysis of plant genomic DNA after bisulphite sequencing. Plant J. *51*, 526–536.

56. Thiel, T., Michalek, W., Varshney, R.K., and Graner, A. (2003). Exploiting EST databases for the development and characterization of gene-derived SSR-markers in barley (*Hordeum vulgare* L.). Theor. Appl. Genet. *106*, 411–422.

57. Marshall, O.J. (2004). PerlPrimer: cross-platform, graphical primer design for standard, bisulphite and real-time PCR. Bioinformatics *20*, 2471–2472.

58. Halitschke, R., Keßler, A., Kahl, J., Lorenz, A., and Baldwin, I.T. (2000). Ecophysiological comparison of direct and indirect defenses in *Nicotiana attenuata*. Oecologia *124*, 408–417.

59. Glawe, G.A., Zavala, J.A., Kessler, A., van Dam, N.M., and Baldwin, I.T. (2003). Ecological costs and benefits correlated with trypsin protease inhibitor production in *Nicotiana attenuata*. Ecology *84*, 79–90.

60. Schuman, M.C., Heinzel, N., Gaquerel, E., Svatos, A., and Baldwin, I.T. (2009). Polymorphism in jasmonate signaling partially accounts for the variety of volatiles produced by *Nicotiana attenuata* plants in a native population. New Phytol. *183*, 1134–1148.

61. Galis, I., Schuman, M.C., Gase, K., Hettenhausen, C., Hartl, M., Dinh, S.T., Wu, J., Bonaventure, G., and Baldwin, I.T. (2013). The use of VIGS technology to study plant-herbivore interactions. Methods Mol. Biol. *975*, 109–137.

62. Gase, K., Weinhold, A., Bozorov, T., Schuck, S., and Baldwin, I.T. (2011). Efficient screening of transgenic plant lines for ecological research. Mol. Ecol. Resour. *11*, 890–902.

63. Frommer, M., McDonald, L.E., Millar, D.S., Collis, C.M., Watt, F., Grigg, G.W., Molloy, P.L., and Paul, C.L. (1992). A genomic sequencing protocol that yields a positive display of 5-methylcytosine residues in individual DNA strands. Proc. Natl. Acad. Sci. USA *89*, 1827–1831.

64. Altschul, S.F., Madden, T.L., Schäffer, A.A., Zhang, J., Zhang, Z., Miller, W., and Lipman, D.J. (1997). Gapped BLAST and PSI-BLAST: a new generation of protein database search programs. Nucleic Acids Res. *25*, 3389–3402.

65. Li, G.Z., Vissers, J.P., Silva, J.C., Golick, D., Gorenstein, M.V., and Geromanos, S.J. (2009). Database searching and accounting of multiplexed precursor and product ion spectra from the data independent analysis of simple and complex peptide mixtures. Proteomics *9*, 1696–1719.

66. Silva, J.C., Gorenstein, M.V., Li, G.Z., Vissers, J.P., and Geromanos, S.J. (2006). Absolute quantification of proteins by LCMS^{E}: a virtue of parallel MS acquisition. Mol. Cell. Proteomics *5*, 144–156.

STAR★METHODS

KEY RESOURCES TABLE

REAGENT or RESOURCE	SOURCE	IDENTIFIER
Bacterial and Virus Strains		
Agrobacterium tumefaciens	[49]	GV3101
Agrobacterium tumefaciens	[50]	LBA4404
Biological Samples		
Nicotiana attenuata	Collection throughout the southwestern USA	N/A
Critical Commercial Assays		
Agencourt Chloropure DNA Isolation Kit	Beckman-Coulter	Cat#A47949
Type-it Microsatellite PCR Kit	QIAGEN	Cat#206243
QIAquick 96 PCR Purification Kit	QIAGEN	Cat#28183
GeneScan 500 ROX dye Size Standard	Thermo-Fisher	Cat#401734
Matchmaker Gold Yeast Two-Hybrid System	Clontech	Cat#630489
EpiTect Bisulfite kit	QIAGEN	Cat#59104
Deposited Data		
N. attenuata genome of UT	*Nicotiana attenuata*	GenBank: MJEQ00000000
N. attenuata genome of AZ	*Nicotiana attenuata*	GenBank: MCOF00000000
NaS-like-RNase1	*Nicotiana attenuata*	GenBank: MH580448
NaS-like-RNase2	*Nicotiana attenuata*	GenBank: MH580449
NaSSK1	*Nicotiana attenuata*	GenBank: MH899921
NaCUL1	*Nicotiana attenuata*	GenBank: MH899922
NaSLF-like1	*Nicotiana attenuata*	GenBank: MH899923
NaSLF-like2	*Nicotiana attenuata*	GenBank: MH899924
NaSLF-like3	*Nicotiana attenuata*	GenBank: MH899925
NaSLF-like4	*Nicotiana attenuata*	GenBank: MH899926
NaSLF-like5	*Nicotiana attenuata*	GenBank: MH899927
NaSLF-like6	*Nicotiana attenuata*	GenBank: MH899928
Other genes used in phylogenetic analysis, see Table S3	This paper	N/A
Experimental Models: Organisms/Strains		
Information of 26 *N. attenuata* accessions, see Table S6	This paper	N/A
Oligonucleotides		
Primer for microsatellite marker: 6FAM-forward: 6FAM-GAGTGTTATGCTGCCTAGAAGAC	This paper	N/A
Primer for microsatellite marker: 6FAM-reverse: CATTTGATCTTGGTGTTCCTCCTC	This paper	N/A
Primer for microsatellite marker: HEX-forward: AGGGTGTTTGGTGAAGATTAGAC	This paper	N/A
Primer for microsatellite marker: HEX-reverse: HEX-GGCTAGATAGTCAGATAGTCCA	This paper	N/A
Primer for microsatellite marker: AT550-forward: AT550-TGGGATGACAATTTATTCAAGCA	This paper	N/A
Primer for microsatellite marker: AT550-reverse: TCTCCGAGTGATGAAATGTG	This paper	N/A
Primers for other experiments, see Table S2	This paper	N/A
Recombinant DNA		
Plasmid for VIGS	[49]	*pTV00*
Plasmid for *EV*/UT	[51]	*pSOL3NC*
Plasmid for *EV*/AZ	[51]	*pRESC2NC*

(*Continued on next page*)

Continued		
REAGENT or RESOURCE	SOURCE	IDENTIFIER
Plasmid for ir*ACO*/UT	[52]	*pRESC5ACO*
Plasmid for ir*SLR1*/UT	This paper	*pSOL8DC3SLR1*
Plasmid for ir*SLR1*/UT	This paper	*pSOL8DCL2SLR2*
Software and Algorithms		
Phylogenetic analysis: MEGA7	[53]	https://www.megasoftware.net/
Graphics and data analysis: R v3.4.4	The Comprehensive R Archive Network (CRAN)	https://cran.r-project.org
Protein quantification: ProteinLynx Global Server (PLGS) v2.5.2	Waters	https://www.waters.com/waters/en_US/ProteinLynx-Global-SERVER
Primer design for PCR after bisulfite assay: Methprimer	[54]	https://www.urogene.org/methprimer/
Data visualization of bisulfite assay: CyMATE	[55]	http://www.cymate.org/
Screening for microsatellite markers: PERL5 script MISA (MIcroSAtellite)	[56]	https://webblast.ipk-gatersleben.de/misa/
Primer selection for microsatellite markers: PerlPrimer	[57]	http://perlprimer.sourceforge.net/
Other		
Phusion High-Fidelity DNA Polymerase	Thermo-Fisher	Cat#F530
Pfu DNA Polymerase	Thermo-Fisher	Cat#EP0501
JumpStart Taq DNA Polymerase	Sigma-Aldrich	Cat#D9307
Pierce Coomassie Plus Assay Kit	Thermo-Fisher	Cat#23236
RNeasy Plant Mini Kit	QIAGEN	Cat#74903
PrimeScript RT Reagent Kit	TaKaRa	Cat#RR037B
qPCR 2X MasterMix for SYBR Assay ROX	Eurogentec	Cat#10-SN2X-03T
NucleoSpin Extract II kit	Macherey-Nagel	Cat#740609
pGEM-T Easy vector system	Promega	Cat#A1360
NucleoSpin Plasmid Kit	Macherey-Nagel	Cat#740588
BigDye Terminator mix v3.1	Applied Biosystems	Cat#4337455

CONTACT FOR REAGENT AND RESOURCE SHARING

Further information and requests for resources and reagents should be directed to and will be fulfilled by the Lead Contact, Ian T. Baldwin (baldwin@ice.mpg.de).

EXPERIMENTAL MODEL AND SUBJECT DETAILS

Plant Material

The *N. attenuata* Utah (UT) and Arizona (AZ) wild-type seeds were originally collected from plants growing in a large natural population near Santa Clara, Utah, USA [58], and a 20-plant population near Flagstaff, Arizona, USA [59] and were inbred for 31 and 22 generations, respectively, in the glasshouse. Seeds of the G2 and G8 accessions were collected in Utah as described in [26, 60]. Additional natural accessions, used as pollen donors, were collected throughout the southwestern United States and inbred for one generation in the glasshouse [48]. Three transgenic lines: empty vector (*pSOL3NC*: *EV*/UT, A-04-266-3; *pRESC2NC*: *EV*/AZ, A-03-364) and *ACC oxidase* silenced lines (*pRESC5ACO*: ir*ACO*/UT, A-03-321-10-1) were previously described [51, 52].

Plant Growth Conditions

All seeds were germinated following the protocol described by Krügel et al. (2002) [50]. Plants were grown under glasshouse conditions (26 ± 1°C; 16h: 8h, light: dark). For the VIGS experiment, plants were grown in climate chambers under a constant temperature of 26°C and 16h:8h (light: dark) light regime and 65% relative humidity [61].

METHOD DETAILS

Mixture Pollinations

Homogeneous pollen mixtures were prepared by collecting equal numbers of freshly matured anthers from each genotype into a sterile Eppendorf tube and thoroughly mixing the dehisced non-sticky pollen. Emasculated flowers were hand-pollinated by gently

applying the homogenized mixture of pollen with a wooden tooth pick. Mean pollen numbers per anther and their viability did not differ among UT, AZ, G2 and G8 accessions as described previously [26].

Constructs

Full-length CDS encoding *NaS-like-RNase1* and *2*, *SLF-like1-6*, *SSK1*, and *CUL1* were amplified by PCR using Pfu DNA polymerase (Thermo-Fisher) with primers listed in Table S2.

For VIGS experiments, ~250 bp sequences of the CDS of *S-like-RNase1*, *2* and *SLF-like1*, *2* and *4* were amplified by PCR using Pfu DNA polymerase (Thermo-Fisher) with primers listed in Table S2. The DNA fragments were cloned into *pTV00* and transformed into *Agrobacterium tumefaciens* GV3101.

For Y2H assays, *NaS-like-RNase1* and *2* (without their signal peptides: amino acids (aa) 1-22), and *NaSSK1* and *PhSSK1* were cloned into *pGADT7* to generate the AD fused constructs; *NaSLF-like1N* (encoding aa 1-60), *NaSLF-like1C* to *6C* (without aa 1-60), and *NaCUL1* were cloned into *pGBKT7* to generate the BD fused genes.

For the silencing of *S-like-RNase1* in UT, DNA fragments identical to those used in the VIGS experiments were cloned into *pSOL8DC3* (GenBank: HQ698853); and for the silencing of *S-like-RNase2* in AZ, DNA fragments identical to those used in the VIGS were cloned into *pSOL8DCL2* (GenBank: HQ698851). Both constructs were transformed into *A. tumefaciens* LBA4404. The transformation protocol was optimized for *N. attenuata* as described previously [50, 62].

VIGS

Leaves of young *N. attenuata* plants were agroinfiltrated with *pBINTRA* and corresponding *pTV00* recombinant plasmids, respectively, according to a published protocol optimized for VIGS in *N. attenuata* [49]. Plants coinfiltrated with *pBINTRA* and *pTV00* were used as control. All VIGS experiments were repeated at least three times.

Yeast-two-hybrid (Y2H) Assay

Y2H was performed using the Matchmaker Gold Yeast Two-Hybrid System (Clontech) according to the manufacturer's manual. Indicated AD and BD control or fusion constructs were co-transformed into yeast strain Y2Hgold and plated on SD –Leu/–Trp selective dropout medium. The transformations grew on QDO (SD –Ade/–His/–Leu/–Trp) plates at 30°C. The plate was photographed 6–7 d after incubation.

Southern Blot Analysis

A total amount of 10 μg genomic DNA was digested overnight at 37°C with 200 U *Eco*RV and *Xba*I (New England Biolabs) in independent reactions. The digested DNA was separated on a 0.8% (w/v) agarose gel for 15 h at 30 Volt. DNA was blotted overnight onto a Gene Screen Plus Hybridization Transfer Membrane (Perkin-Elmer) using the capillary transfer method. For gene copy number analysis of *NaS-like-RNase1* and *2*, gene-specific probes identical to the fragments used in the VIGS and RNAi silencing constructs were amplified (primer pairs listed in Table S2) and radiolabeled with [α-32P] dCTP (Perkin-Elmer) using the Rediprime II DNA Labeling System (GE Healthcare) according to the manufacturer's instructions. For transgene insertion number analysis, the *hpt*II gene was amplified with the primer pair HYG1-18 (5′-CCGGATCGGACGATTGCG-3′) and HYG2-18 (5′-CTGACGGACAATGGCCGC-3′) [4] and digoxigenin-labeled with DIG-dUTP (Roche) using the DIG High Prime DNA labeling System (Roche) according to the manufacturer's instructions. The blot was washed twice at high stringency (0.1 × SSC and 0.5% SDS for 20 min).

Bisulfite Genomic Sequencing

DNA methylation was analyzed by bisulfite sequencing [63]. The bisulfite conversion was performed using the EpiTect Bisulfite kit (QIAGEN) according to the manufacturer's instructions. A total of 1 μg stylar genomic DNA was converted with the following temperature program 95°C for 5 min, 60°C for 25 min, 95°C for 5 min, 60°C for 85 min, 95°C for 5 min, 60°C for 175 min. The target sequences were amplified from the converted DNA with 0.05 U μL^{-1} JumpStart Taq DNA Polymerase with the provided reaction buffer (Sigma-Aldrich), 200 μM dNTP Mix (Fermentas) and 0.5 μM of the primers listed in Table S2. Primers were designed using the Methprimer software (http://www.urogene.org/methprimer/) [54]. Cycle parameters used were 94°C for 1 min followed by 35 cycles with 94°C for 30 s, 53°C for 30 s, 72°C for 30 s and a final step with 72°C for 10 min. PCR products were purified by gel electrophoresis, excised and purified with the NucleoSpin Extract II kit (Macherey-Nagel) and cloned into the *pGEM-T Easy* vector system (Promega). Plasmids of individual picked clones were isolated with the NucleoSpin Plasmid Kit (Macherey-Nagel). Sequencing was performed with the BigDye Terminator mix v3.1 (Applied Biosystems) supplemented with 5% dimethyl sulfoxide (DMSO). Sequences were manually trimmed and data analysis performed with the online tool CyMATE (http://cymate.org/) [55]. A minimum of 5 individual clones per PCR reaction and 10 independent PCR reactions of each natural accession were analyzed.

Plant Transformation and Transgenic Line Screening

Plant transformation was performed by *A. tumefaciens*-mediated gene transfer as previously described [50]. In brief, *Agrobacterium tumefaciens* LBA4404 carrying the required binary plant transformation vector was grown overnight at 28°C in 8 mL of liquid YEP medium containing 50 mg L^{-1} Kanamycin (Duchefa, https://www.duchefa-biochemie.com/), 5 mg L^{-1} Rifampicin (Duchefa) and 300 mg L^{-1} Streptomycin (Duchefa). The bacteria were washed twice and resuspended in the same volume of Murashige-Skoog medium (MS medium, Duchefa) containing 0.02 mg L^{-1} indole-3-acetic acid (IAA, Duchefa). Explant hypocotyls from 9-10 day-old

seedlings were cut by a scalpel into 3 mm long pieces. Before each cut the tip of the scalpel was dipped into the bacterial solution. The explant hypocotyls were co-cultivated with the bacteria in darkness for 3 days. The transformed hypocotyls were regenerated in the following three steps on specific phytagel-based medium [50] containing 20 mg L^{-1} hygromycin B (Duchefa) for selection and 125 mg L^{-1} ticarcillin disodium/clavulanate potassium (timentin, Duchefa) as antibacterial agent: 1) 14-21 days of callus induction (MS medium; 30 g L^{-1} sucrose; 3 g L^{-1} phytagel; 0.02 mg L^{-1} IAA; 1 mg L^{-1} 6-benzylaminopurine, BAP, Duchefa); 2) 14-21 days of shoot regeneration (MS medium; 30 g L^{-1} sucrose; 3 g L^{-1} phytagel; 0.5 mg L^{-1} BAP); 3) 14-21 days of shoot maturation (MS medium; 30 g L^{-1} sucrose; 3 g L^{-1} phytagel). For root regeneration, transgenic plants were cultured on rooting medium (1/2 MS medium; 6 g L^{-1} plant agar) without antibiotics for at least 21 days. Following the regeneration steps, plants were grown on soil in Magenta boxes (https://www.bio-world.com/) for 4 weeks and then were transferred to 2-L pots and grown for flowering and seed production.

For germination seeds were sterilized for 5 min with a 2% (w/v) aqueous solution of sodium dichloroisocyanuric acid (DCCS, Sigma-Aldrich) and treated for 1 h with 0.1 M gibberellic acid (GA3, Sigma-Aldrich) in 50 × diluted liquid smoke solution (House of Herbs). At least 60 seedlings per plant were germinated on Gamborg's B5 Medium (GB5 medium, Duchefa) supplemented with 35 mg L^{-1} hygromycin B (Duchefa) and incubated in a growth chamber (Percival; day 16 h 26°C, night 8 h 24°C). After 10 days of germination, the segregation rate (% of sensitive seedlings) was determined and resistant seedlings transferred to the glasshouse under constant temperature and light conditions (day 16 h 26-28°C, night 8 h 22-24°C). Two independent transgenic lines for each construct were used in this study: ir*NaS-like-RNase1*/UT (A-17-091-7 and A-17-094-5) and ir*NaS-like-RNase2*/AZ (A-17-058-3 and A-17-161-8).

Identification and Selection of Microsatellite Markers

The 2.5 Gbp genome of a single *N. attenuata* plant of ecotype UT was sequenced at the Dresden-concept Genome Center (Dresden, Germany) using PacBio technology. By running 192 SMRT cells with RSII P6/C4 chemistry, 15.2 M reads with 63x genome coverage were created. The complete *N. attenuata* genome was *de novo* assembled only from this PacBio data by DNA nexus, Mountain View, California, USA. The assembly comprised 1.97 Gbp, consisting of 8916 contigs and had an N50 contig length of 393 Kbp.

This assembly was screened for microsatellite sequences using the PERL5 script MISA (MIcroSAtellite) [56]. With the chosen settings [definition (unit_size, min_repeats): 1-500 2-15 3-15 4-10 5-5 6-5; interruptions (max_difference_between_2_SSRs): 100; GFF: true] 49,435 *N. attenuata* microsatellite sequences, each consisting of repeated units of 2 to 5 base pairs and the 100 bp flanking sequences on both sides, were extracted.

1,872 of the extracted sequences starting with different repeated base pairs (AG: 101; AT: 199; CC: 570; CT: 128; GA: 774; TT: 100) and with different lengths [2 bp: 261; 3 bp: 528; 4 bp: 5; 5 bp: 339; 6 bp: 685) and thus about equally representing the different types of microsatellite sequences found, were chosen for BLASTN [64] alignments against the above described *N. attenuata* genome assembly. BLASTN was done with standard settings, active low complexity filter and BLOSUM-62 matrix.

For the design of primers that would allow the PCR amplification of a single and specific microsatellite fragment from *N. attenuata* genomic DNA, the BLASTN alignments were filtered to identify the extracted microsatellite sequences that best fulfill the following conditions: one flanking sequence should only appear once and with an alignment score $\geq$ 80, all other hits should have an alignment score of $\leq$ 50; the other flanking sequence first should have at least one, but as few as possible hits with an alignment score $\geq$ 80, and second should have as few as possible hits with an alignment score of < 80. By applying these conditions, 145 microsatellites were identified for primer design.

100 primer pairs for genotyping PCRs were designed using the program PerlPrimer [57] with the following settings: primer Tm 57-63°C, difference 3°C, primer length 20-24 bases. The primers were synthesized and tested in PCRs with genomic DNA from *N. attenuata* ecotypes UT and AZ as templates. 17 primer pairs that amplified a strong, single product with both templates and at the expected size with gDNA from the *N. attenuata* ecotype UT were chosen for genotyping. For this, one primer of each primer pair was synthesized and labeled with a fluorescent dye (HEX, 6FAM or AT550). Oligonucleotide synthesis was performed by Sigma-Aldrich, Steinheim, Germany, except for the oligonucleotides labeled with AT550, which were synthesized at Eurofins Genomics, Ebersberg, Germany. To simplify the genotyping that would distinguish the 14 pollen donors, primer pairs numbered 4, 24 and 100 were selected and mixed for one round of PCR (Table S2).

QUANTIFICATION AND STATISTICS

Progeny Paternity Assessment of Matured Seeds

In order to genotype paternity of seeds produced from binary mixture pollinations, the paternity was determined from 24 seeds randomly selected from the total seeds (~10%) of each capsule, which predicted the exact paternity ratio for all seeds within a capsule as described in [26]. DNA extracted from two-week-old seedlings (Agencourt Chloropure DNA Isolation Kit, Beckman-Coulter) was used as PCR templates. PCR products of *NaTPI* primers (Table S2) showed different sizes among UT, AZ, G2 and G8 (Figure S1E). Fragment size differences were also displayed after PCR (by *NaS-like-RNase2* dCAPS primers, Tables S2 and S4) and digestion by *Tsp*45I (Figure S1F).

For genotyping seed paternity in mixture pollinations of 14 pollen donors, the paternity was determined from ~50 seeds randomly selected from the total seeds (~20%) of each capsule. DNA extracted from two-week-old seedlings (Agencourt Chloropure DNA Isolation Kit, Beckman-Coulter) was used as PCR template. Multiplex PCR reactions, using a Type-It microsatellite PCR kit (QIAGEN), were performed with 50 ng DNA and a primer pair mixture (primer pair 4, 24 and 100). Approximately 250 ng purified

PCR product (QIAquick 96 PCR purification kit, QIAGEN) was mixed with 0.5 μL GeneScan 500 ROX size standard (Thermo-Fisher) to resolve the sizes of amplified microsatellite markers on an ABI 3100 genetic analyzer (Applied Biosystems). Allele size and genotypes were determined using the GENEMAPPER software version 3.7 (Applied Biosystems). Correspondence between allele size and genotypes of both maternal and paternal genotypes is listed in Table S6.

Protein Quantification: Protein Extraction, Spiking with Internal Standard and Precipitation

100 mg fresh mature styles (2-3 h before anthesis) were collected, ground under liquid nitrogen and incubated in 0.5 mL protein extraction buffer (50 mM Tris, 50 mM NaCl, 50 mM EDTA and 10% glycerol, pH 7.6) on ice for 1 h. After centrifugation for 10 min at 13000x g at 4°C, the supernatant was transferred to a fresh tube. The protein concentration was measured using Bradford assay (Thermo-Fisher). Protein extracts were spiked with bovine serum albumin (BSA) (Sigma-Aldrich) used as an internal standard. One pmol of BSA was added to 1 μg of total soluble protein. Proteins were precipitated by the addition of trichloroacetic acid (TCA) to a final concentration of 10% (w/v) overnight at –20°C. After centrifugation for 15 min at 4°C with 13000x g, the precipitates were washed twice with 90% acetone, centrifuged again at 4°C with 13000x g for 5 min and dried. Protein pellets were dissolved in 40 μL of 100 mM ammonium bicarbonate, heated to 90°C for denaturation of proteins and cooled on ice. Methanol was added to a final concentration of 60% (v/v). Tryptic digestion was performed at 37°C overnight using sequencing grade porcine trypsin (Promega) at a trypsin/protein ratio of 1:30. Tryptic peptides were dried down in a vacuum centrifuge and dissolved to a final concentration of 200 ng μL^{-1} in water containing 0.1% formic acid.

Protein Quantification: LC-MS^E Analysis

200, 300, 400 or 500 ng of each sample were injected into an UPLC M-class system (Waters) online coupled to a Synapt G2-si mass spectrometer equipped with a T-WAVE-IMS device (Waters). Samples were first on-line preconcentrated and desalted using a UPLC M-Class Symmetry C18 trap column (100Å, 180 μm x 20 mm, 5 μm particle size) at a flow rate of 15 $\mu L\ min^{-1}$ of 0.1% aqueous formic acid (FA). Peptides were eluted onto a ACQUITY UPLC HSS T3 analytical column (100Å, 75 μm x 200 mm, 1.8 μm particle size) and separated at a flow rate of 350 $nL\ min^{-1}$ using the following gradient of acetonitrile in 0.1% aqueous FA: from 2% to 65% over 65 min, from 65% to 80% over 10 min, increased to 95% over 5 min, held at 95% for 2 min and decreased to 2% over 3 min, followed by re-equilibration for 15 min.

The mass spectrometer was operated in positive ESI and V-mode with a resolving power of > 20000 full width at half height FWHM. A 200 fmol μL^{-1} solution of human Glu-Fibrinopeptide B in 0.1% aqueous FA/acetonitrile (1:1 v/v) was infused at a flow rate of 1 $\mu L\ min^{-1}$ through the reference sprayer every 45 s to compensate for mass shifts in MS and MS/MS fragmentation mode.

Data were collected using MassLynx v4.1 software (Waters) under data-independent acquisition that utilizes alternating scanning in low (MS) and elevated energy (MS^E) mode. In low energy mode, data were collected at a constant collision energy of 4 eV. In elevated energy (MS^E) mode, collision energy was ramped from 20 to 45 eV. MS and MS^E data were acquired over 0.5 s intervals in the mass range of 50-2000 m/z.

Each sample was measured in duplicate or triplicate.

Protein Quantification: Data Processing and Protein Identification

The acquired LC-MS^E data were processed using ProteinLynx Global Server (PLGS) version 2.5.2 (Waters) to generate product ion spectra for database searching according to the Ion Accounting algorithm described by Li et al. [65]. The processed data were searched against a protein database containing *Petunia* and *Nicotiana* species (downloaded from NCBI on 20th June 2018) combined with a database containing common contaminants (human keratins and trypsin). The database search was performed at a False Discovery Rate (FDR) of 2% and the following search parameters were applied: minimum numbers of fragments per peptide: 3, peptides per protein: 1, fragments per protein: 7; and a maximum number of missed tryptic cleavage sites: 1. Searches were restricted to tryptic peptides with a fixed carbamidomethylation of cysteines.

After protein identification, intensities of the three most abundant peptides (*Hi3* approach [66]) of the internal standard (BSA) were used to calculate the amounts of identified proteins. The *N. attenuata* elongation factor protein was used as internal control.

Quantitative RT-PCR

Total RNA was isolated using the RNeasy Plant Mini Kit (QIAGEN), and 1000 ng of total RNA were reverse transcribed using the PrimeScript RT-qPCR Kit (TaKaRa). At least four independent biological replicates were collected and analyzed. RT-qPCR was performed on the Stratagene 500 MX3005P using a SYBR Green reaction mix (Eurogentec). The primers used for mRNA detection of target genes by RT-qPCR are listed in Table S2. The mRNA of *N. attenuata elongation factor* was used as internal control.

Current Biology, Volume *29*

Supplemental Information

Mate Selection in Self-Compatible Wild Tobacco Results from Coordinated Variation in Homologous Self-Incompatibility Genes

Han Guo, Rayko Halitschke, Natalie Wielsch, Klaus Gase, and Ian T. Baldwin

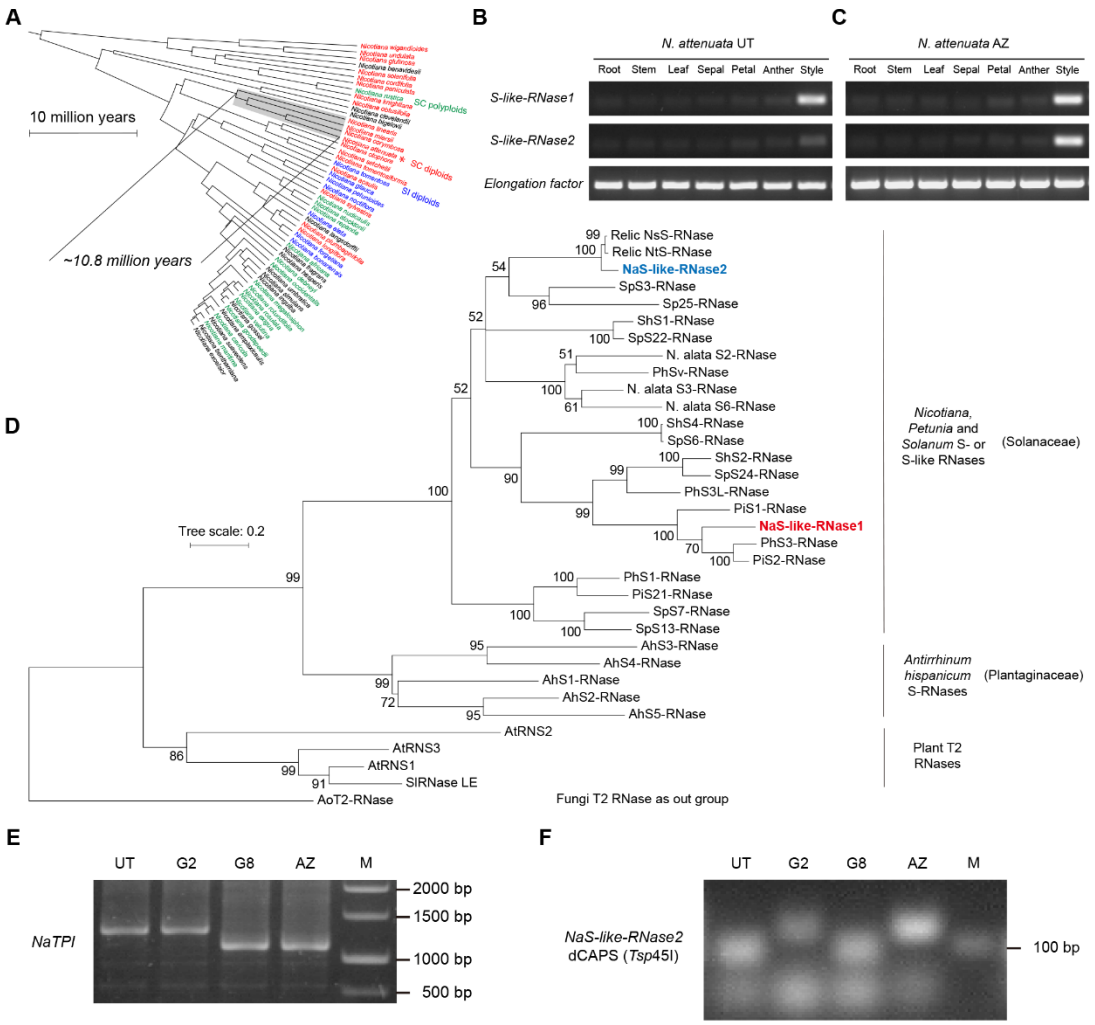

Figure S1. Phylogenetic Relationships, Ploidy, and Breeding System of 55 *Nicotiana* Species; Tissue-Specific Expression and Phylogenetic Analysis of NaS-like-RNases; *NaTPI* and *NaS-like-RNase2* dCAPS Markers that Distinguish Different Accessions. Related to Figures 1, 3, S3 and Table S3. (A) The figure is modified from [S1] and [S2]. Branch lengths were obtained with penalized likelihood smoothing, implemented in *r8s* [1]. Red, self-compatible diploids; blue, self-incompatible diploids; green, self-compatible polyploids; black, unknown mating system and ploidy. *N. attenuata* and its closely related species are shaded in grey. (B and C) Transcript accumulation of *S-like-RNase1* and *2* in (B) UT and (C) AZ examined by RT-PCR. Total RNA was extracted from seven tissues as indicated. The synthesized cDNAs were used as templates in RT-PCR. *Nicotiana attenuata elongation factor* (*NaEF*) was used as a positive control. (D) Phylogenetic tree of S- and S-like-RNases. Numbers on branches indicate the bootstrap percentage values calculated from 1000 replicates, and only values greater than 50% are shown. Self-compatible species: *At*, *Arabidopsis thaliana*; *Ns*, *Nicotiana sylvestris*; *Nt*, *Nicotiana tabacum*; *Na*, *Nicotiana attenuata*; *Sl*, *Solanum lycopersicum*. Self-incompatible species: *Sp*, *Solanum peruvianum*; *Sh*, *Solanum habrochaites*; *Ph*, *Petunia x hybrida*; *Pi*, *Petunia inflata*; *Ah*, *Antirrhinum hispanicum*. Fungi *Aspergillus oryzae* T2 RNase was used as an out group for the phylogenetic analysis. (E) PCR products of the trypsin proteinase inhibitor (*NaTPI*) gene in four accessions. (F) PCR products of *S-like-RNase2* flanking sequences were digested by

*Tsp*45I. Genomic DNA was extracted from leaves of different accessions as template for PCR.

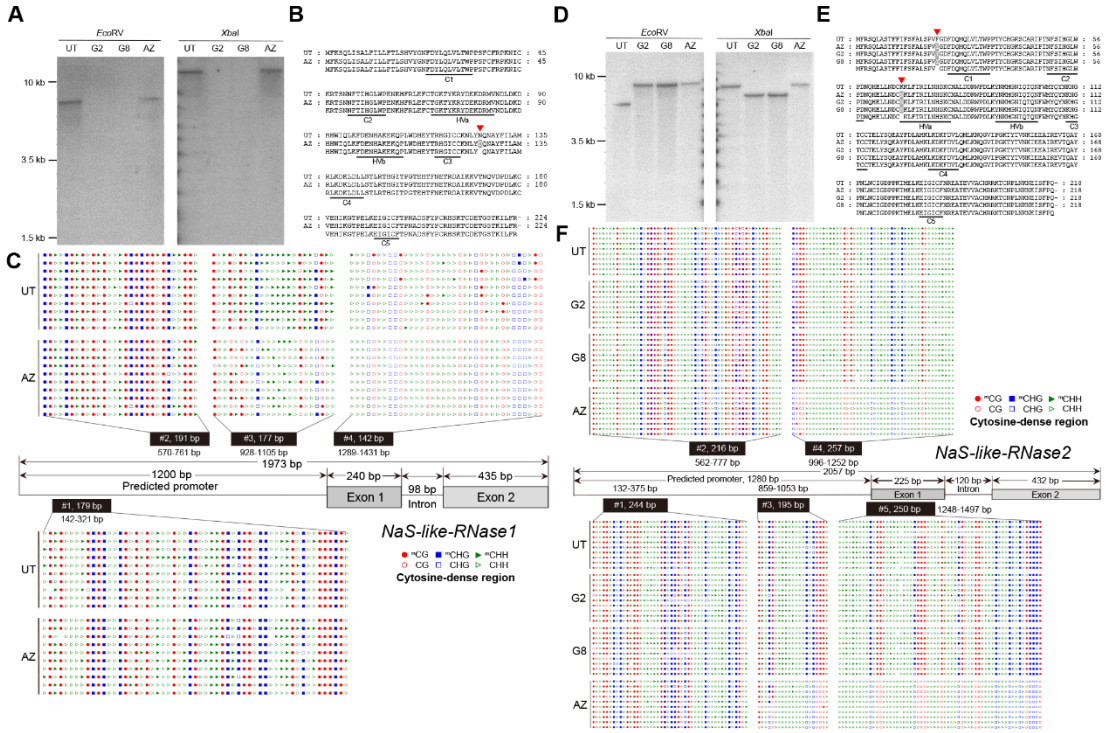

Figure S2. Comparison of Copy Number, Amino Acid Sequence and Cytosine Methylation of *NaS-like-RNase1* and *2* in Four Natural Accessions. Related to Figure 2 and Table S5. (A and D) Southern blot analysis to identify *NaS-like-RNase1* (A) and *2* (D) copy number. Genomic DNA isolated from leaf tissue was separately digested by *Eco*RV or *Xba*I and probed by the 240 bp (A) or 245 bp (D) fragment, which is used for both VIGS constructs and the quantification of gene silencing. The primers amplifying the fragments are listed in Table S2. Molecular weights in base pairs (bp) are shown on the left side of the blots. (B and E) Amino acid sequence alignment of NaS-like-RNase1 (B) and 2 (E) alleles. Different residues are highlighted by red triangles. The conserved regions C1 through C5 and hypervariable regions HVa and HVb are underlined. (C and F) Cytosine methylation frequencies in the predicted promoter and first exon of *S-like-RNase1* (C) and *2* (F) are shown. Four (C) or five (F) black boxes represent CpG-dense regions for methylation analysis. The middle panel illustrates the spatial distribution of the CpG-dense regions within the predicted promoter and first exon. DNA for bisulfite assays was isolated from styles. The top and bottom panels are graphical representations of cytosine methylation corresponding to the CpG-dense regions. Filled symbols indicate cytosine methylation; empty symbols indicate a lack of methylation. Red circles represent CG sites, blue squares represent CHG sites and green triangles represent CHH sites, H = A, T or C. Analysis was performed with CyMATE. The DNA elements shown are not to scale.

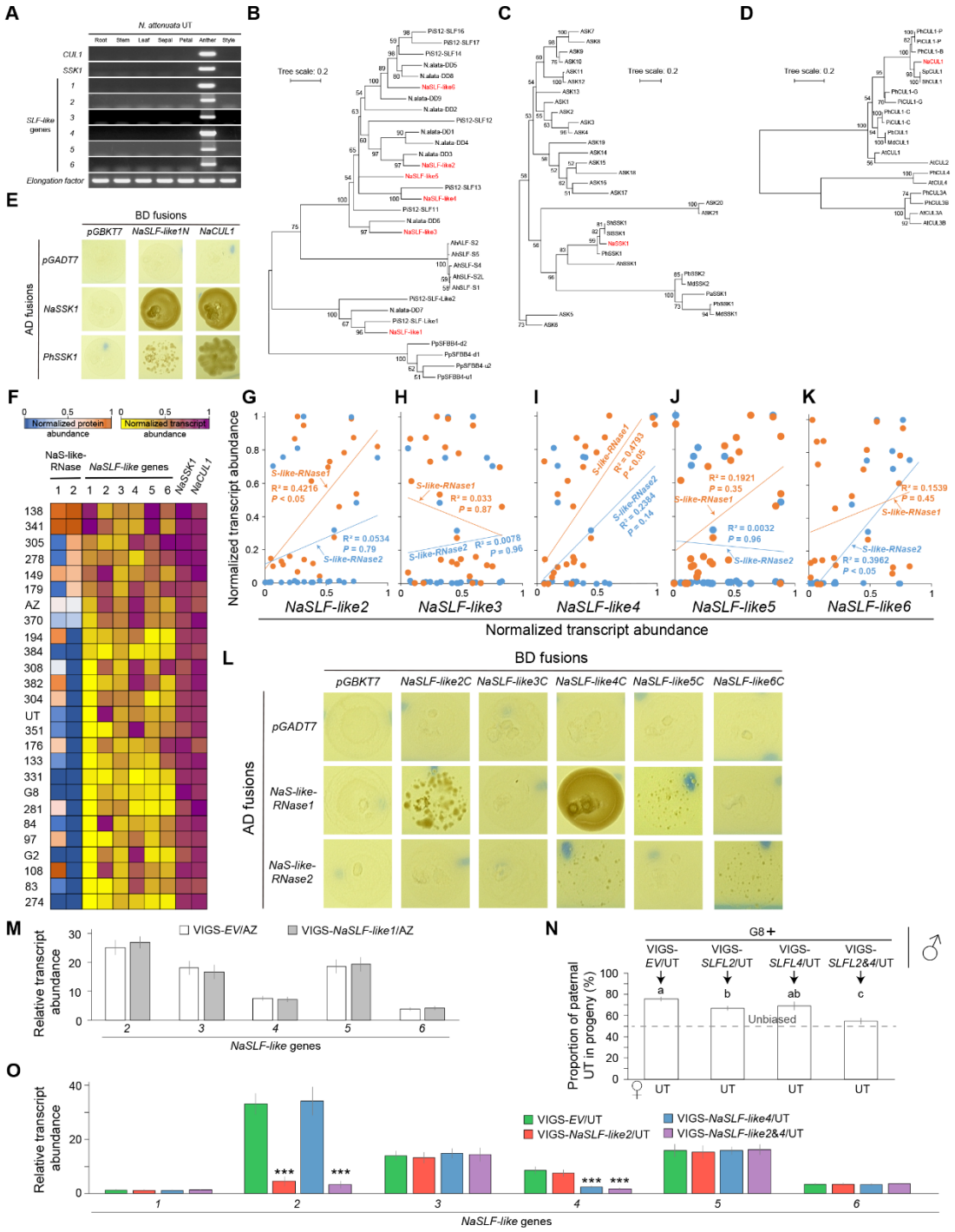

Figure S3. Tissue-Specific Expression, Phylogeny and Protein-Protein Interaction Analysis of SCF$^{SLF\text{-}like1}$ Complexes; Correlation and Protein-Protein Interaction Analysis among *S-like-RNases* and *SLF-like2-6*; Silencing Specificity in VIGS-*NaSLF-like* Transgenic Lines and Redundancy of *NaSLF-like2* and *4* Function in Mate Selection. Related to Figure 3, Tables S1 and S3. (A) Transcript accumulation pattern of *NaCUL1*, *SSK1* and *SLF-like1-6* in UT examined by RT-PCR. Total RNA was extracted from seven tissues as indicated. The synthesized cDNAs were used as templates in RT-PCR. The *NaEF* gene was used as a positive control. (B to D) Phylogenetic trees of (B) SLF or SLF-like proteins, (C) SKP1-like or SLF-interacting SKP1 proteins and (D) Cullin1 proteins are

presented. Numbers on branches indicate the bootstrap percentage values calculated from 1000 replicates: only values greater than 50% are shown. *Ah*, *Antirrhinum hispanicum*; *At*, *Arabidopsis thaliana*; *Md*, *Malus domestica*; *Na*, *Nicotiana attenuata*; *N. alata*, *Nicotiana alata*; *Pa*, *Prunus avium*; *Pb*, *Pyrus bretschneideri*; *Pi*, *Petunia inflata*; *Ph*, *Petunia hybrida*; *Pp*, *Pyrus pyrifolia*; *Sh*, *Solanum habrochaites*; *Sl*, *Solanum lycopersicum*; *Sp*, *Solanum peruvianum*. (E and L) Yeast cells containing different combinations of BD fusions and AD fusions (E: BD: *NaSLF-like1N*, encoding N-terminus of 1-60 amino acids, and *NaCUL1*, AD: *NaSSK1* and *PhSSK1*; L: *NaSLF-like2-6C*, encoding C-terminus without 1-60 amino acids, AD: *S-like-RNase1* and *2*) were tested for their growth on -Leu/-Trp/-His/-Ade dropout media. Empty vector *pGBKT7* and *pGADT7* were used as negative controls. (F) The normalized protein abundance (relative to NaEF, and normalized as $X' = X/X_{max}$) of NaS-like-RNase1 and 2, together with the normalized transcript abundance (relative to *NaEF* and normalized as $X' = X/X_{max}$) of *SLF-like1-6*, *SSK1* and *CUL1* were quantified in 26 *N. attenuata* natural accessions. (G-K) Correlation analyses among normalized transcript abundance of *NaS-like-RNases* and (G) *NaSLF-like2*; (H) *SLF-like3*; (I) *SLF-like4*; (J) *SLF-like5*; (K) *SLF-like6* are shown. *S-like-RNase1* and *2* data are displayed in orange or blue, respectively. (M) *NaSLF-like2* to *6* relative transcript abundance (mean ± SE, n=4, relative to *NaEF*) was quantified in pollen of empty vector (VIGS-*EV*/AZ) and *NaSLF-like1*-silenced (VIGS-*NaSLF-like1*/AZ) AZ transgenic lines. (N) The percentage of seeds sired by paternal UT genotype (mean ± SE, n=4) in progeny of mixed pollinations. Emasculated flowers of UT plants were pollinated with equal pollen mixtures from G8 and empty vector (VIGS-*EV*/UT), *NaSLF-like2*-silenced (VIGS-*SLFL2*/UT), *NaSLF-like4*-silenced (VIGS-*SLFL4*/UT), *NaSLF-like2* and *4*-co-silenced (VIGS-*SLFL2&4*/UT) UT transgenic lines, respectively. Each replicate represents a capsule from an independent pollination. Different letters indicate significant differences in a Tukey-corrected *post-hoc* test following a one-way ANOVA ($P < 0.05$). The dotted line indicates the unbiased seed set percentage for a 1:1 pollen mixture applied to the stigma. (O) *NaSLF-like1* to *6* relative transcript abundance (mean ± SE, n=4, relative to *NaEF*) was quantified in pollen of empty vector (VIGS-*EV*/UT), *NaSLF-like2*-silenced (VIGS-*NaSLF-like2*/UT), *NaSLF-like4*-silenced (VIGS-*NaSLF-like4*/UT), *NaSLF-like2* and *4*-co-silenced (VIGS-*NaSLF-like2&4*/UT) UT transgenic lines. Asterisks indicate significant differences (*$P < 0.05$; **$P < 0.01$; ***$P < 0.001$; Student's *t*-test).

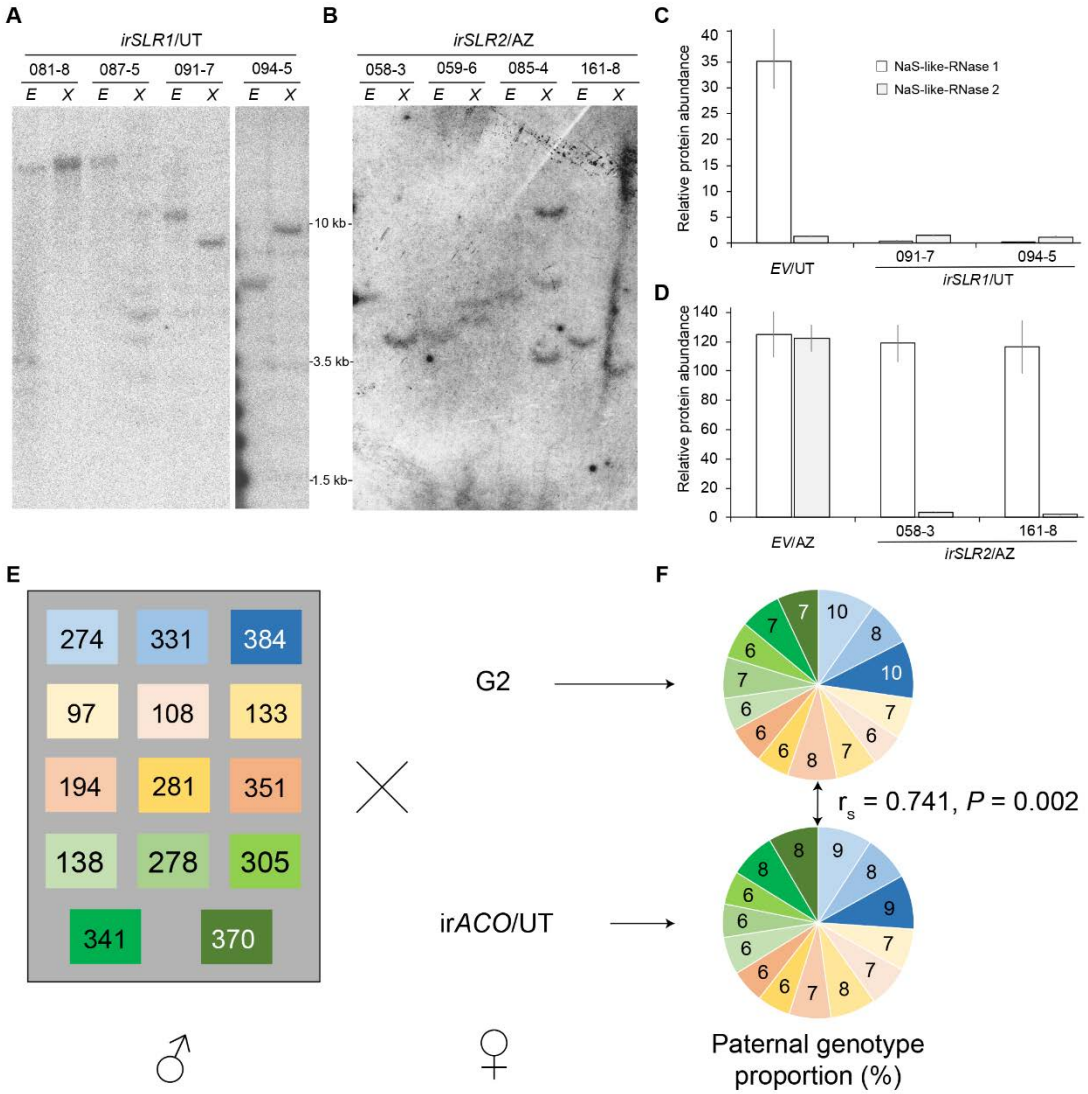

Figure S4. Southern Blot and Silencing Efficiency Analysis of *NaS-like-RNase* RNAi Transgenic Lines; No Significant Difference of Progeny Paternity between G2 and ir*ACO*/UT Flowers in Mixture Pollinations. Related to Figure 4 and Table S1. (A and B) Southern blot analysis was performed to detect the T-DNA copy number in transgenic lines silenced in (A) *NaS-like-RNase1* in the UT background (ir*SLR1*/UT) and (B) *NaS-like-RNase2* in the AZ background (ir*SLR2*/AZ). Genomic DNA was isolated from homozygous plants of the T_2 generation and digested overnight in separate reactions with *Eco*RV (*E*) or *Xba*I (*X*). A DIG-labeled fragment of the hygromycin resistance gene (*hptII*) served as probe. The blot indicates the presence of T-DNA insertion for transgenic lines: A-17-081-8, A-17-087-5, A-17-091-7, A-17-094-5, A-17-058-3, A-17-059-6, A-17-085-4 and A-17-161-8. The fragment size from the DNA markers is indicated. (C and D) Relative protein abundance (mean ± SE, n=3, relative to NaEF) of S-like-RNases in (C) *EV*/UT and two ir*SLR1*/UT or in (D) *EV*/AZ and two ir*SLR2*/AZ transgenic lines were quantified by mass spectrometry in styles. (E) Schematic representation of mixture pollinations with 14 non-self pollen genotypes. G2 or ir*ACO*/UT maternal genotypes (♀) were pollinated with equal-number mixed pollen loads containing equal contributions from 14 pollen donors (♂). (F) Pie charts (and numbers within slices) indicate percentage (mean of 3 replicates, each replicate represents a capsule resulting from

an independent pollination) of each paternal genotype of seeds fertilized in the equal-pollen grain mixture pollination. Slice colors correspond to the colors shown in (E). From each capsule, at least 50 seeds were germinated. Genomic DNA was extracted from two-week-old seedlings and analyzed for paternity by three microsatellite markers optimized to genotype these particular *N. attenuata* accessions. Spearman's correlations (r_s) quantify the consistency of mate selection between G2 and ir*ACO*/UT flowers.

Genetic background	Wild-type or transgenic line	Target gene	Related to figure	Relative protein abundance (to NaEF)	
				S-like-RNase 1	S-like-RNase 2
UT	WT	-	1 & 2	31.07	1.29
	VIGS	Empty vector	1	34.55	2.17
		SLR1		0.74	1.99
	RNAi	Empty vector	4	35.11	1.37
		SLR1 (091-7)		0.43	1.49
		SLR1 (094-5)		0.32	1.26
AZ	WT	-	1 & 2	118.28	112.97
	VIGS	Empty vector	1	113.26	115.97
		SLR1		6.03	112.80
		SLR2		121.67	14.11
	RNAi	Empty vector	4	124.96	122.37
		SLR2 (58-3)		118.97	3.26
		SLR2 (161-8)		116.37	2.23
G2	WT	-	1 & 2	N.D.	0.12
G8				N.D.	0.054
274	WT	-	2 & 4	0.013	0.017
331				N.D.	0.57
384				8.89	0.99
97				173.07	0.23
108				221.54	0.068
133				35.15	0.65
194				191.89	3.06
281				135.59	0.52
351				31.95	0.95
138	WT	-	2 & 4	209.99	234.08
278				33.75	176.75
305				24.22	189.44
341				218.89	233.79
370				60.17	74.07
83	WT	-	2	28.54	0.041
84				25.36	0.33
138				209.99	234.08
176				154.31	0.91
179				26.02	163.28
304				161.71	1.59
351				31.95	0.95

382	193.22	1.61

Table S1. Natural Accessions and Transgenic Lines with Corresponding Relative Protein Abundances of NaS-like-RNases. Related to Figures 1, 2, 4, S4 and STAR Methods.

Gene	Sequence (5' to 3')	Purpose
SLR1-F	ATGTTTAAGTCACAGCTAATATC	Cloning, RT-PCR
SLR1-R	TTATCGGAACAAAATCTTCGTG	Cloning, RT-PCR
SLR2-F	ATGTTTAGATCGCAGCTCGTG	Cloning, RT-PCR
SLR2-R	TCATTGTGGAAAACTAATTTCATTCTTG	Cloning, RT-PCR
SLFL-F	ATGAAAGAGGTGGACGGTCAAAG	Cloning, RT-PCR
SLFL-R	TTAGGACCACTTCTCTCTCTCTTTC	Cloning, RT-PCR
SSK1-F	ATGGCAACCGAAGGCAAGAAA	Cloning, RT-PCR
SSK1-R	CTAATTAACAGTATCATCAATTTCAG	Cloning, RT-PCR
CUL1-F	ATGGAAGAGACTGAGGAGAAG	Cloning, RT-PCR
CUL1-R	TTAGGCAATGTACTTGTACGTG	Cloning, RT-PCR
SLR1-RT-F	CACATTTAACGAAACCAGAGATGCC	RT-qPCR
SLR1-RT-R	TTTATATGTTCGACGCACTTGAGGT	RT-qPCR
SLR2-RT-F	AGCGTATCCTAACCTCAATTGCATT	RT-qPCR
SLR2-RT-R	GTTGCCTCTCGGTTGAAACAGA	RT-qPCR
SLFL1-RT-F	AGCGGGTGATAATTGGATCGTTTC	RT-qPCR
SLFL1-RT-R	ACTCTTGCACGGTTCAATGTCTAAG	RT-qPCR
SLFL2-RT-F	GCTTCCTCCTATTGAATATCCGTTA	RT-qPCR
SLFL2-RT-R	ATTTGAGTTCCTTTACTTCATCGGA	RT-qPCR
SLFL3-RT-F	CGTGTGGGTCAACAGTTTCC	RT-qPCR
SLFL3-RT-R	AACACTTCCCATCGTAGCCA	RT-qPCR
SLFL4-RT-F	TGTCATAGCCTCGCAGTCTTAGATAA	RT-qPCR
SLFL4-RT-R	CGTTTCTTGTATTGGGCTACTCTCC	RT-qPCR
SLFL5-RT-F	TGGAGGGATCATCTGTTGTTTCTTC	RT-qPCR
SLFL5-RT-R	TGAACTCCTTGACTTCTTCCGAATG	RT-qPCR
SLFL6-RT-F	CCTCGTAGTCTTGGATGAGTCTCTA	RT-qPCR
SLFL6-RT-R	GCACACCTTCATTATCCAAATTTCCA	RT-qPCR
SSK1-RT-F	CGAGGACAAGGACAAGGACA	RT-qPCR
SSK1-RT-R	TCAGCTGCAGATTGACAACA	RT-qPCR
CUL1-RT-F	TGTCTTGTGCGTATAATGAAAGCCA	RT-qPCR
CUL1-RT-R	TTTGCTCAACTGCTCAACACACT	RT-qPCR
EF-RT-F	CCACACTTCCCACATTGCTGT	RT-PCR, RT-qPCR
EF-RT-R	CGCATGTCCCTCACAGCAAAAC	RT-PCR, RT-qPCR
TPI-F	CTTGTAAGCAATGTGGAACATGCAGATGCC	Molecular marker
TPI-R	TTAGGAAACAGCAACCCTAGACTTCTGGAG	Molecular marker
SLR2-dCAPS-F	AAAGAAAATTCTACTTTCCTTACACTTTGTGA	Molecular marker
SLR2-dCAPS-R	CCAAGATTCGATTACACGGG	Molecular marker
SLR1-VIGS-F	ATGTTTATGGGAACTTTGATTATC	VIGS, Southern blot
SLR1-VIGS-R	TTCATCGAACTTCAATTGAATCC	VIGS, Southern blot
SLR2-VIGS-F	GCATATTTTGATCTTGCCATG	VIGS, Southern blot
SLR2-VIGS-R	GTCTTACGTCGATGACAAGC	VIGS, Southern blot
SLFL1-VIGS-F	CGGGTTTGACCCCAACACTAATG	VIGS
SLFL1-VIGS-R	GGTTTGTTCCACGCCAATGAAATG	VIGS
SLFL2-VIGS-F	CCACTCATCGGTCCTTGTAA	VIGS

SLFL2-VIGS-R	TAAGAGGATCCCAAAACAC	VIGS
SLFL4-VIGS-F	CAACTCACTGGTCCTTGCAATG	VIGS
SLFL4-VIGS-R	AGGGGGGTTCCCCGTAAAC	VIGS
SLR1-Pro-F	CTCTCTCTCTCTCTCTCTCTC	Promoter cloning
SLF2-Pro-F	ACTGGGCGAAAATTGGGATTGAC	Promoter cloning
SLR1-CDR1-F	TTTGTTTAGTTATGTAATGGTTATAAAGAG	Bisulfite sequencing
SLR1-CDR1-R	CCCAAACTAATTATTAAAATAATTTATATT	Bisulfite sequencing
SLR1-CDR2-F	AAGGTTTATGTGATAATGATAGGAGG	Bisulfite sequencing
SLR1-CDR2-R	AATACAATTCTAATTACAAAAATAAATCTC	Bisulfite sequencing
SLR1-CDR3-F	GTTTATAATTGTTTTGGTATTAATTATTT	Bisulfite sequencing
SLR1-CDR3-R	TATTAACCTAAATTCTTTCCCTTCC	Bisulfite sequencing
SLR1-CDR4-F	TGGGAATTTTGATTATTTGTAATTTG	Bisulfite sequencing
SLR1-CDR4-R	ACTTAAAAAAACACTCTATACTTTTTCATC	Bisulfite sequencing
SLR2-CDR1-F	AGAATGTGGTATATTTAAAGTGGTATAATT	Bisulfite sequencing
SLR2-CDR1-R	ACCTTTAACACATAAAATTTTCTTTACC	Bisulfite sequencing
SLR2-CDR2-F	TTATTTTTTTTATATTTTATGATTGTGTTT	Bisulfite sequencing
SLR2-CDR2-R	AAATATAACTCAATTTTAATAACAACTCC	Bisulfite sequencing
SLR2-CDR3-F	TTAGATTATATTTGATTTTATGTTAAGGTA	Bisulfite sequencing
SLR2-CDR3-R	ATTAAATATCTATCAATTTCATCTTTTAAT	Bisulfite sequencing
SLR2-CDR4-F	ATTATTTATATTTTATTGTGAATTTAGTTA	Bisulfite sequencing
SLR2-CDR4-R	ATTTTAATATTAAAACCACTCATCTCTTAT	Bisulfite sequencing
SLR2-CDR5-F	ATTTTAATGAGAAAAGAGTGTTATATATAG	Bisulfite sequencing
SLR2-CDR5-R	TAAAATAATATTATAATTATACCAAAATTC	Bisulfite sequencing
SLR1-AD-F	AACTTTGATTATCTGCAACTTGTTTTAAC	Y2H
SLR1-AD-R	TCGGAACAAAATCTTCGTGCTG	Y2H
SLR2-AD-F	GATTTCGACCAAATGCAACTCG	Y2H
SLR2-AD-R	TTGTGGAAAACTAATTTCATTCTTG	Y2H
SLFL1-C-BD-F	TTCACTCTGTTTAAGCGCTTCATC	Y2H
SLFL1-C-BD-R	GGACCACTTCTCTCTCTCTTTC	Y2H
SLFL1-N-AD-F	ATGAAAGAGGTGGACGGTCAAAG	Y2H
SLFL1-N-AD-R	ATTTGAAAGACAATCATGATTG	Y2H
SSK1-AD-F	ATGGCAACCGAAGGCAAGAAAATG	Y2H
SSK1-AD-R	ATTAACAGTATCATCAATTTCAG	Y2H
PhSSK-AD-F	ATGGCATCAGAAAAGAAAATG	Y2H
PhSSK-AD-R	ATTGACAGTATCATCAATTTC	Y2H
CUL1-BD-F	ATGGAAGAGACTGAGGAGAAG	Y2H
CUL1-BD-R	GGCAATGTACTTGTACGTGTTCG	Y2H

Table S2. DNA Primers Used in This Study. Primers for microsatellite markers see Key Resources Table and STAR Methods. Related to Figures 1, 2, 3, 4, S1, S2, S3, S4 and STAR Methods.

Gene	Species	GenBank accession number
AhS1-RNase	*Antirrhinum hispanicum*	CAD29435.1
AhS2-RNase	*Antirrhinum hispanicum*	Q38716.1
AhS3-RNase	*Antirrhinum hispanicum*	CAC41959.1
AhS4-RNase	*Antirrhinum hispanicum*	Q38717.1
AhS5-RNase	*Antirrhinum hispanicum*	CAA65318.1
AoT2-RNase	*Aspergillus oryzae*	EIT82935.1
AtRNS1	*Arabidopsis thaliana*	NP_178399.1
AtRNS2	*Arabidopsis thaliana*	NP_030524.1
AtRNS3	*Arabidopsis thaliana*	NP_564264.1
N. alata_S2-RNase	*Nicotiana alata*	P04007.1
N. alata_S3-RNase	*Nicotiana alata*	AAB07492.1
N. alata_S6-RNase	*Nicotiana alata*	AAB40028.1
PhS1-RNase	*Petunia x hybrida*	AAA60465.1
PhS2-RNase	*Petunia x hybrida*	Q40875.1
PhS3L-RNase	*Petunia x hybrida*	AJ271065.1
PhSv-RNase	*Petunia x hybrida*	BAA76513.1
PiS1-RNase	*Petunia inflata*	AAA33726.1
PiS2-RNase	*Petunia inflata*	AAG21384.1
PiS21-RNase	*Petunia inflata*	AAG40753.1
ShS1-RNase	*Solanum habrochaites*	AIG62994.1
ShS2-RNase	*Solanum habrochaites*	AIG62995.1
ShS4-RNase	*Solanum habrochaites*	AIG62997.1
SlRNase LE	*Solanum lycopersicum*	NP_001234195.1
SpS3-RNase	*Solanum peruvianum*	CAA53666.1
SpS6-RNase	*Solanum peruvianum*	CAA81334.1
SpS7-RNase	*Solanum peruvianum*	CAA81333.1
SpS13-RNase	*Solanum peruvianum*	BAA04147.1
SpS22-RNase	*Solanum peruvianum*	BAC00930.1
SpS24-RNase	*Solanum peruvianum*	BAC00932.1
SpS25-RNase	*Solanum peruvianum*	BAC00933.1
AhSLF-S2	*Antirrhinum hispanicum*	CAC33010.1
AhSLF-S2L	*Antirrhinum hispanicum*	CAC33011.1
AhSLF-S4	*Antirrhinum hispanicum*	CAD56661.1
AhSLF-S1	*Antirrhinum hispanicum*	CAD56663.1
AhSLF-S5	*Antirrhinum hispanicum*	CAD56664.1
N. alata-DD1	*Nicotiana alata*	ABR18781.1
N. alata-DD2	*Nicotiana alata*	ABR18782.1
N. alata-DD3	*Nicotiana alata*	ABR18783.1
N. alata-DD4	*Nicotiana alata*	ABR18784.1
N. alata-DD5	*Nicotiana alata*	ABR18785.1
N. alata-DD6	*Nicotiana alata*	ABR18786.1
N. alata-DD7	*Nicotiana alata*	ABR18787.1
N. alata-DD8	*Nicotiana alata*	ABR18788.1

N. alata-DD9	*Nicotiana alata*	ABR18789.1
PpSFBB4-u2	*Pyrus pyrifolia*	BAJ52223.1
PpSFBB4-u1	*Pyrus pyrifolia*	BAJ52224.1
PpSFBB4-d1	*Pyrus pyrifolia*	BAG07418.1
PpSFBB4-d2	*Pyrus pyrifolia*	BAJ52227.1
PiS12-SLF-Like2	*Petunia inflata*	AIK66494.1
PiS12-SLF11	*Petunia inflata*	AIK66455.1
PiS12-SLF-Like1	*Petunia inflata*	AIK66490.1
PiS12-SLF14	*Petunia inflata*	AIK66470.1
PiS12-SLF12	*Petunia inflata*	AIK66460.1
PiS12-SLF13	*Petunia inflata*	AIK66465.1
PiS12-SLF16	*Petunia inflata*	AIK66480.1
PiS12-SLF17	*Petunia inflata*	AIK66485.1
PhSSK1	*Petunia x hybrida*	ACT35733.1
ShSSK1	*Solanum habrochaites*	AIG62999.1
SlSSK1	*Solanum lycopersicum*	AIG62966.1
PaSSK1	*Prunus avium*	XP_021834044.1
AhSSK1	*Antirrhinum hispanicum*	ABC84197.1
PbSSK1	*Pyrus x bretschneideri*	CCH26217.1
PbSSK2	*Pyrus x bretschneideri*	CCH26218.1
MdSSK1	*Malus domestica*	NP_001281293.1
MdSSK2	*Malus domestica*	CCH26220.1
ASK1	*Arabidopsis thaliana*	NP_565123.1
ASK2	*Arabidopsis thaliana*	NP_568603.1
ASK3	*Arabidopsis thaliana*	NP_565604.1
ASK4	*Arabidopsis thaliana*	NP_564105.1
ASK5	*Arabidopsis thaliana*	NP_567091.1
ASK6	*Arabidopsis thaliana*	NP_566978.1
ASK7	*Arabidopsis thaliana*	NP_566693.1
ASK8	*Arabidopsis thaliana*	NP_566692.1
ASK9	*Arabidopsis thaliana*	NP_566694.1
ASK10	*Arabidopsis thaliana*	NP_566695.1
ASK11	*Arabidopsis thaliana*	NP_567959.1
ASK12	*Arabidopsis thaliana*	NP_567967.1
ASK13	*Arabidopsis thaliana*	NP_567090.1
ASK14	*Arabidopsis thaliana*	NP_565296.1
ASK15	*Arabidopsis thaliana*	NP_566773.1
ASK16	*Arabidopsis thaliana*	NP_565297.1
ASK17	*Arabidopsis thaliana*	NP_565467.1
ASK18	*Arabidopsis thaliana*	AAD32873.1
ASK19	*Arabidopsis thaliana*	NP_565295.1
ASK20	*Arabidopsis thaliana*	NP_001078065.1
ASK21	*Arabidopsis thaliana*	NP_567113.1
PhCUL1-B	*Petunia x hybrida*	BAW00384.1

PhCUL1-C	*Petunia x hybrida*	BAW00386.1
PhCUL1-G	*Petunia x hybrida*	BAW00387.1
PhCUL3A	*Petunia x hybrida*	BAW00389.1
PhCUL3B	*Petunia x hybrida*	BAW00390.1
PhCUL4	*Petunia x hybrida*	BAW00391.1
PhCUL1-P	*Petunia x hybrida*	BAO58961.1
PiCUL1-C	*Petunia inflata*	ABB77428.1
PiCUL1-G	*Petunia inflata*	ABB77429.1
PiCUL1-P	*Petunia inflata*	AHF49537.1
SpCUL1	*Solanum pennellii*	NP_001310370.1
PbCUL1	*Pyrus x bretschneideri*	NP_001289253.1
AtCUL1	*Arabidopsis thaliana*	NP_567243.1
AtCUL2	*Arabidopsis thaliana*	NP_171797.2
AtCUL3A	*Arabidopsis thaliana*	NP_174005.1
AtCUL3B	*Arabidopsis thaliana*	NP_177125.3
AtCUL4	*Arabidopsis thaliana*	NP_568658.1
MdCUL1	*Malus domestica*	XP_008390685.1
ShCUL1	*Solanum habrochaites*	AIG63002.1

Table S3. GenBank ID of Genes for Phylogenetic Analysis. Related to STAR Methods, Figure S1 and Figure S3.

Position of SNPs	Accession			
	UT	AZ	G2	G8
-726*	C	T	T	T
-606	T	G	G	G
62	T	A	A	A
162	G	A	A	A
204	G	T	T	T

Table S4. SNPs of the Predicted Promoter (1280 bp) and ORF of *NaS-like-RNase2* in UT, AZ, G2 and G8. Related to Figures 2, S1, S2 and STAR Methods. Start codon was taken as position 0. The SNP with asterisk was used in dCAPS markers in Figure S1F.

	Cytosine-dense region	Methylation type	Methylation rate (%) (mean ± SE, n=10)		*t*-test (*P* value)
			UT	AZ	
NaS-like-RNase1	1	CG	98.75 ± 1.25	100 ± 0	0.33
		CHG	96 ± 2.21	95 ± 2.24	0.75
		CHH	22.04 ± 2.85	27.4 ± 3.42	0.24
	2	CG	99.5 ± 0.5	100 ± 0	0.33
		CHG	100 ± 0	98 ± 2	0.42
		CHH	34.97 ± 6.06	32.5 ± 5.62	0.77
	3	CG	92 ± 3.27	62 ± 8.14	0.003
		CHG	85 ± 7.64	40 ± 10	0.002
		CHH	59.38 ± 7.05	14.4 ± 1.875	7.99E-06
	4	CG	17.5 ± 3.82	0 ± 0	0.00023
		CHG	7.15 ± 2.38	0 ± 0	0.0077
		CHH	2.85 ± 0.78	0 ± 0	0.0017
NaS-like-RNase2	1	CG	94 ± 3.4	96 ± 1.63	0.60
		CHG	85.56 ± 4.4	91.11 ± 3.23	0.32
		CHH	18.21 ± 3.14	14.81 ± 1.83	0.36
	2	CG	98.57 ± 1.429	100 ± 0	0.33
		CHG	84.45 ± 4.74	68.69 ± 5.44	**0.045**
		CHH	16.59 ± 1.69	7.575 ± 1.98	**0.0044**
	3	CG	100 ± 0	24 ± 4	**2.33E-13**
		CHG	93.33 ± 4.44	9.99 ± 5.09	**3.25E-10**
		CHH	27.69 ± 3.84	2.31 ± 1.17	**5.83E-06**
	4	CG	99.9 ± 0.1	0 ± 0	**3.75E-44**
		CHG	82.5 ± 7.5	0 ± 0	**2.02E-09**
		CHH	10.14 ± 1.24	0 ± 0	**1.77E-07**
	5	CG	97.27 ± 1.39	0 ± 0	**2.16E-23**
		CHG	90 ± 3.08	0 ± 0	**1.25E-16**
		CHH	19.49 ± 1.34	0 ± 0	**2.15E-11**

Table S5. Comparison of Cytosine Methylation in Four Cytosine-Dense Regions of *NaS-like-RNase1* between UT and AZ or Five Cytosine-Dense Regions of *NaS-like-RNase2* between G2 and AZ, Respectively. Related to Figures 2 and S2.

Accession	Allele size (bp) of PCR products amplified by different primer pairs			Latitude	Longitude
	Primer pair with 6FAM	Primer pair with HEX	Primer pair with AT550		
UT	181	163 and 513	225	N37°19'36.26"	W113°57'53.05"
AZ	169	147 and 495	223	N35°12'56.07"	W111°27'41.29"
G2	178	124 and 473	197	N37°04'33.53"	W113°49'58.74"
97	140	124 and 473	209	N37°21'35.24"	W113°56'38.68"
108	175	150 and 498	203	N37°13'52.699"	W113°50'37.113"
133	160	150 and 498	209	N37°06'12.5"	W113°49'36.6"
138	181	150 and 498	225	N37°8'19.58"	W114°1'35.10"
194	137	124 and 473	205	N37°20'22.52"	W114°2'40.86"
274	178	150 and 498	209	N37°21'07.103"	W114°05'50.298"
278	181	124 and 473	237	N37°21'02.580"	W114°05'53.661"
281	175	163 and 513	219	N37°19'35.48"	W113°57'38.28"
305	134	147 and 495	ND	N37°45'19.61"	W118°35'41.82"
331	178	124 and 473	197	N37°13'15.83"	W113°48'20.86"
341	181	153 and 502	209	N37°9'45.30"	W114°0'58.52"
351	117	124 and 473	183	N37°17'09.1"	W114°07'31.5"
370	137	150 and 498	189	N37°9'1.30"	W113°47'43.36"
384	175	163 and 513	215	N37°14'27.05"	W113°49'36.71"
G8	N/A	N/A	N/A	N37°04'33.53"	W113°49'58.74"
83	N/A	N/A	N/A	N37°19'35.48"	W113°57'38.28"
84	N/A	N/A	N/A	N37°19'35.48"	W113°57'38.28"
149	N/A	N/A	N/A	N35°12'56.07"	W111°27'41.29"
176	N/A	N/A	N/A	N37°16'38.65"	W113°53'35.18"
179	N/A	N/A	N/A	N37°21'1.04"	W113°57'5.17"
304	N/A	N/A	N/A	N37°20'22.52"	W114°2'40.86"
308	N/A	N/A	N/A	N37°13'5.50"	W113°48'24.25"
382	N/A	N/A	N/A	N37°14'27.05"	W113°49'36.71"

Table S6. Characterization of Three Microsatellite Markers and full GPS Coordinates for the collection sites of *N. attenuata* Natural Accessions. Related to Figures 2, 4, S2, S4 and STAR Methods. Not detected, ND; not available, N/A.

	Pollen tube growth rate			
	H1: detrimental effect		H2: promoting effect	
pollen tube	SLR (+) style	SLR (-) style	SLR (+) style	SLR (-) style
SLFL (+)	a	a	a	b (b<a)
SLFL (-)	b (b<a)	a	b	a

Table S7. Predicted Results of Pollen Tube Growth Rates for Two Alternative Mechanistic Hypotheses. Related to Figure 5. Predictions for different combinations of pollen and styles with high (+) or experimentally reduced (-) SLF-like (SLFL) and S-like-RNase (SLR) protein abundance, respectively. SLFL and SLR proteins are known to interact directly and are functional in the mate selection process. Predicted results of pollen tube growth rates are shown for two alternative mechanistic hypotheses: H1) S-like-RNases might have a detrimental effect on unfavored pollen tubes; H2) the interactions between S-like-RNase and SLF-like promotes or protects the growth of favored pollen tubes.

Supplemental References

S1. Goldberg, E.E., Kohn, J.R., Lande, R., Robertson, K.A., Smith, S.A., and Igic, B. (2010). Species selection maintains self-incompatibility. Science *330*, 493-495.

S2. Robertson, K., Goldberg, E.E., and Igic, B. (2011). Comparative evidence for the correlated evolution of polyploidy and self-compatibility in Solanaceae. Evolution *65*, 139-155.